END
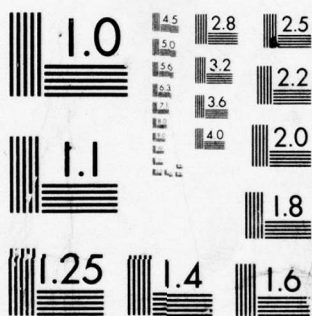
DATE
FILMED
12-76

MICROCOPY RESOLUTION TEST CHART
NATIONAL BUREAU OF STANDARDS-1963-A

AFAPL-TR-76-56

FG.

(12)

TRANSIENT RESPONSE OF A CANTILEVERED PLATE TO IMPACT USING HOLOGRAPHIC INTERFEROMETRY AND FINITE ELEMENT TECHNIQUES
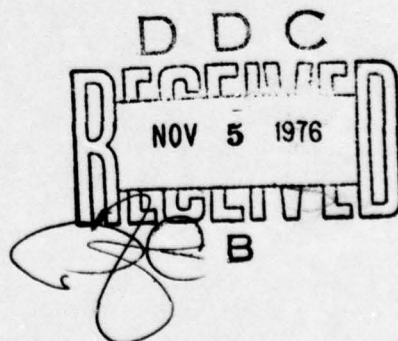
PROPULSION BRANCH
TURBINE ENGINE DIVISION

AUGUST 1976

TECHNICAL REPORT AFAPL-TR-76-56
FINAL REPORT FOR PERIOD 1 JANUARY 1976 TO 1 AUGUST 1976

D D C
RECEIVED
NOV 5 1976
B

AIR FORCE AERO PROPULSION LABORATORY
AIR FORCE WRIGHT AERONAUTICAL LABORATORIES
AIR FORCE SYSTEMS COMMAND
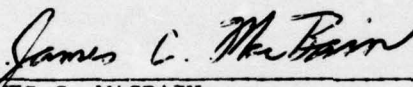WRIGHT-PATTERSON AIR FORCE BASE, OHIO 45433

This technical report has been reviewed and is approved for
publication.

DR. JAMES C. MACBAIN
Project Engineer

FOR THE COMMANDER

L.J. GERSHON, Tech Area Manager
Propulsion Branch
Turbine Engine Division

(9) Final rept. 1 Jan–1 Aug 76

REPORT DOCUMENTATION PAGE		READ INSTRUCTIONS BEFORE COMPLETING FORM
1. REPORT NUMBER (14) AFAPL-TR-76-56	**2. GOVT ACCESSION NO.**	**3. RECIPIENT'S CATALOG NUMBER**
4. TITLE (and Subtitle) Transient Response of a Cantilevered Plate to Impact Using Holographic Interferometry and Finite Element Techniques		**5. TYPE OF REPORT & PERIOD COVERED** Final Report 1 January 76 – 1 August 76
		6. PERFORMING ORG. REPORT NUMBER
7. AUTHOR(s) (10) James C. MacBain		**8. CONTRACT OR GRANT NUMBER(s)**
9. PERFORMING ORGANIZATION NAME AND ADDRESS Air Force Aero Propulsion Laboratory Wright-Patterson AFB, Ohio 45433		**10. PROGRAM ELEMENT, PROJECT, TASK AREA & WORK UNIT NUMBERS** 646100 306612 3066 30661221
11. CONTROLLING OFFICE NAME AND ADDRESS Air Force Aero Propulsion Laboratory Wright-Patterson AFB, Ohio 45433		**12. REPORT DATE** (11) August 76
		13. NUMBER OF PAGES 64 (12) 71 P.
14. MONITORING AGENCY NAME & ADDRESS(if different from Controlling Office)		**15. SECURITY CLASS. (of this report)** Unclassified
		15a. DECLASSIFICATION/DOWNGRADING SCHEDULE

16. DISTRIBUTION STATEMENT (of this Report)

Approved for Public Release, Distribution Unlimited

17. DISTRIBUTION STATEMENT (of the abstract entered in Block 20, if different from Report)

18. SUPPLEMENTARY NOTES

19. KEY WORDS (Continue on reverse side if necessary and identify by block number)

1. Transient Response   5. Cantilevered Plate
2. Impact
3. Finite Element Analysis
4. Holography

20. ABSTRACT (Continue on reverse side if necessary and identify by block number)

This report covers work carried out at AFAPL's Turbo Structures Research Laboratory (TSRL) on the transient structural response of an isotropic cantilevered plate subjected to normal impact by a ballistic pendulum. The program was a combined experimental/analytical effort. The experimental portion utilized a pulsed ruby laser to obtain holographic interferograms of the plate's deformation following impact. The analytical portion of the work consisted of mathematically modelling the plate using finite element techniques and studying the model's response to impact using the general purpose finite element program, NASTRAN.

DD FORM 1 JAN 73 **1473** EDITION OF 1 NOV 65 IS OBSOLETE

011 570

FOREWORD

This report covers work carried out at AFAPL's Turbo Structures Research Laboratory (TSRL) on the transient structural response of an isotropic cantilevered plate subjected to normal impact by a ballistic pendulum. The effort was intended as a vehicle for evaluating the methods of pulsed laser holography and finite element analysis as they relate to the study of transient structural dynamics. This is an area which bears directly on the problem of foreign object damage to turbine engine components.

The program was a combined experimental/analytical effort. The experimental portion utilized a pulsed ruby laser to obtain holographic interferograms of the plate's deformation following impact. The analytical portion of the work consisted of mathematically modelling the plate using finite element techniques and studying the model's response to impact using the general purpose finite element program, NASTRAN.

The work was performed in the Turbine Engine Division of the Air Force Aero Propulsion Laboratory, Air Force Systems Command, Wright-Patterson Air Force Base, Ohio under Project 3066, Task 12, and Work Unit 21. The effort was conducted by Dr. James C. MacBain of the Propulsion Branch.

The author is indebted to Mr. Bruce Tavner for his very competent technical assistance in the laboratory and to Miss Helen Davis for typing the manuscript.

AFAPL-TR-76-56

TABLE OF CONTENTS

LIST OF ILLUSTRATIONS

LIST OF ILLUSTRATIONS (CONT'D)

AFAPL-TR-76-56

SECTION I

INTRODUCTION

Foreign object damage in both military and civilian turbine engines is a seldom but serious problem both in terms of cost and safety. For example, the Air Force Inspection and Safety Center states that 2816 birdstrikes have been reported Air Force-wide between 1966 and 1973. These birdstrikes resulted in a loss of 7 lives, 14 aircraft, and a cost to the Air Force of $74 million dollars. These figures serve to underline the fact that there is a definite need for both basic and applied research in the area of impact-tolerant turbine engine blading. More sophisticated design tools and impact theories are required. In this vein, this report covers work carried out at AFAPL's Turbo Structures Research Laboratory (TSRL) on the transient structural response of an isotropic canti-levered plate subjected to normal impact by a ballistic pendulum. The program was a combined experimental/analytical effort. The experimental portion utilized a pulsed ruby laser to obtain holo-graphic interferograms of the plate's deformation following impact. The analytical portion of the work consisted of mathematically modelling the plate using finite element techniques and studying the model's response to impact using the general purpose finite element program, NASTRAN.

The specific aims of this research effort were threefold. First, the advantages and disadvantages of using pulsed laser holography for transient structural analysis were studied. Second, it was intended

1

to use the experimental pulsed holography results as a verification
of results obtained analytically using the computer program, NASTRAN.
Finally, the research effort served to provide knowledge of and
experience with pulsed laser holography - information that will be
useful in future TSRL research efforts.

SECTION II

SUMMARY OF RESULTS

An aluminum cantilevered plate measuring 3"x7"x.1875" was struck with a ballistic pendulum consisting of a .65" diameter steel ball attached to a wire on a pivot. The resulting plate response was measured for a specified time after impact by double exposure holographic interferometry using a pulsed ruby laser. The plate's normal displacement was experimentally determined for times after impact ranging from 2 to 33µs. Photographs of the double exposure holograms from these tests are shown in Figures 4.1-4.5. The normal displacement based on four of the test runs (times after impact of 4, 6, 12, and 18µs) is shown as a function of plate geometry in Figures 4.10-4.13.

The flexural wave velocity was computed from the holographic interferograms by plotting the plate wave position versus time after impact and was found to be C_f = .102 in/µs. This is in good agreement with the theoretical Rayleigh surface wave velocity of .112 in/µs - a difference of 8.5%.

A parallel numerical study was conducted using the finite element computer program NASTRAN to compute the cantilevered plate's transient response. The results were in good agreement with the experimental findings. The plate's normal displacement based on finite element analysis is shown plotted in Figures 4.10-4.13 as a function of plate geometry (dashed lines). Contour plots of the plate's normal displacement for different times after impact were also generated by NASTRAN and are shown in Figures 5.3-5.5.

The study demonstrated the feasibility and utility of using pulsed laser holography to study transient structural response. In addition, it provided increased confidence and experience in the use of NASTRAN's transient analysis capability.

SECTION III

EXPERIMENTAL SET UP AND PROCEDURE

3.1 Physical Configuration

The test piece for the experimental portion of the impact analysis program was a 6061-T6 aluminum plate measuring 12" in length, 3" in width, and 3/16" thick. The plate was fixed between two steel blocks having a total weight of 33 lbf such that it was cantilevered and had a free length of 7". The weight of the cantilevered portion of the plate was .394 lbf. The plate and jig are shown in Figure 3.1.

The plate was impacted normally by a steel ball weighing .043 lbf at a point lying on its long axis and located 3" above its fixed end as shown in Figure 3.1. The ball was soldered to a thin wire that in turn was fixed to a pivot located a distance above the impact point forming what is known as a ballistic pendulum. The impact sequence was initiated by suspending the steel ball from an electromagnet which was then switched off allowing the ball to swing down and strike the plate. Just prior to impact, the ball interrupted a continuous wave laser beam passing behind the plate (see Figure 3.2) causing a photo diode to transmit a 10V signal that initiated the pulsed laser firing sequence. The timing and electronics involved in the pulsed laser firing sequence will be addressed in more detail in a later section.

The optical set up for making the hologram is also shown in Figure 3.2. The placement of the optics is typical of that used to make transmission holograms with an off-axis holographic set up, and the reader is referred
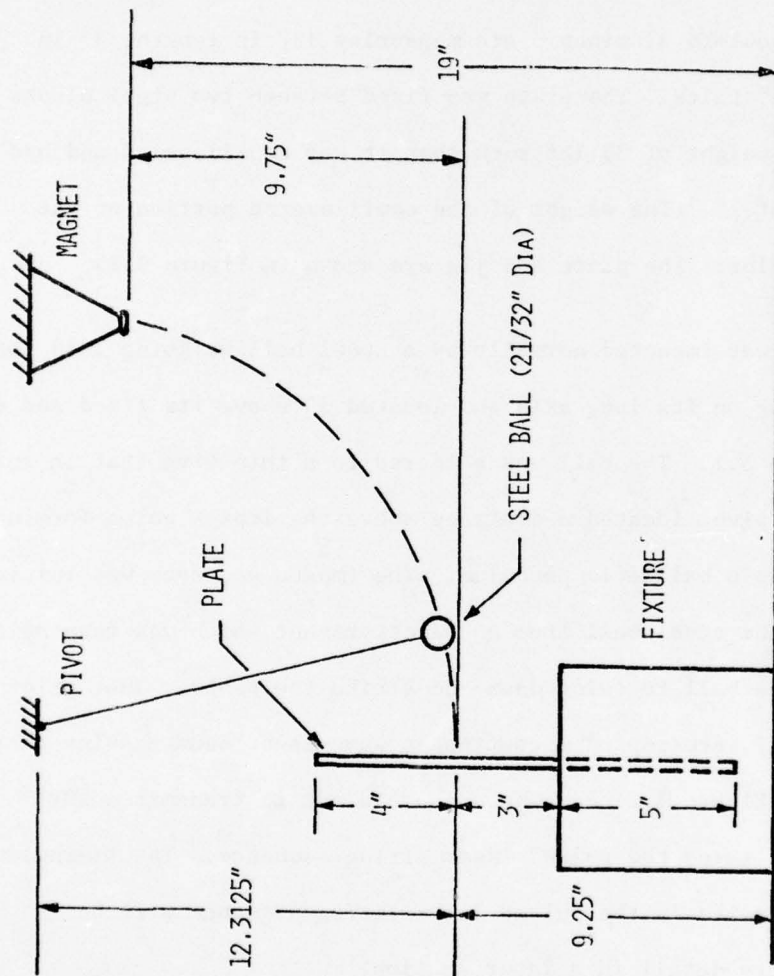
Figure 3.1 - Cantilever Plate and Pendulum Geometry

6
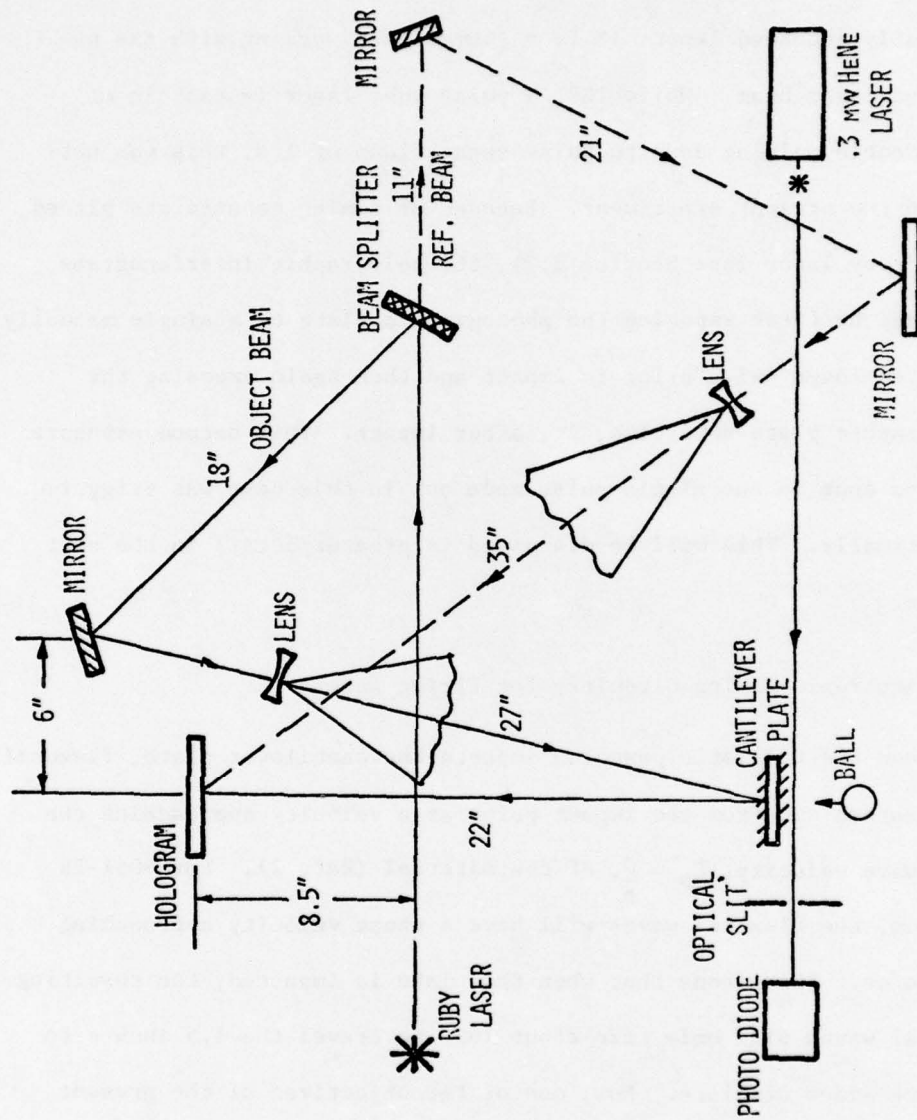
Figure 3.2 - Experimental Set-up for Making Holographic Interferograms

to Reference 1 for details. The holograms were made using a pulsed ruby laser (Apollo Model 22HD). The laser puts out 2.5 joules/pulse, 20-50ns in width, which necessitates the use of dielectric mirrors and doubly concaved lenses (F.L. = -40mm) when working with the un-expanded laser beam. While TSRL's pulse ruby laser is capable of rapid double pulsing down to pulse separations of 1μs, this was not done in the present experiment. Because of timing constraints placed on the ruby laser (see Section 3.2), the holographic interferograms were made by first exposing the photographic plate to a single manually initiated laser pulse prior to impact and then again exposing the photographic plate some time, Δt, after impact. This second exposure was also done in the single pulse mode but in this case was triggered automatically. This will be discussed in greater detail in the next section.

3.2 Electronic Timing Circuitry for Firing Laser

When the ballistic pendulum impacts the cantilever plate, flexural waves spread out from the impact point at a velocity approaching the shear wave velocity, $C_S = \dfrac{G}{\rho}$, of the material (Ref. 2). For 6061-T6 aluminum, the flexural waves will have a phase velocity approaching .114 in/μs. This means that when the plate is impacted, the resulting flexural waves will only take about 16μs to travel the 1.5 inches to the free sides of plate. Now, one of the objectives of the present study was to analyze the plate deformation just after impact, i.e., at times after impact prior to significant wave reflection off the plate's boundaries. For acceptable results, this places an upper

bound on the time for firing the second laser pulse of about 30µs (wave reflection will occur off the closest free edges of the plate at $t \doteq 16\mu s$). This in turn places some constraints on the firing sequence for the ruby laser since, as shown in Figure 3.3, the ruby laser can fire only after 200µs have elapsed - the amount of time necessary for the flash lamps to energize. This is true for either the single pulse, as in the present case, or the double pulse mode of operation. Hence, in order for the laser to lase automatically at some time after impact in the 0-30µs range, it would have to be triggered (signal sent to Master Sync) at some time prior to impact. This was done using a timing delay oscilloscope (Tektronix 535) as follows.

Prior to making the double exposure hologram, the time that it took the ball to go from the trigger laser beam to the plate was measured by an electronic counter. This is shown as T_{AC} in Figure 3.4. This distance traversed by the ball in going from A to C was approximately 1 inch and T_{AC} was typically in the .02 second range (20,000µs). Upon specifying the time after plate impact to be observed, T_{IMPT}, and utilizing the fact that Pulse #2 of the laser fires at 1000µs into the firing sequence, the delay time, T_{AB}, was determined from the relationship:

$$T_{AB} = T_{AC} + T_{IMPT} - 1000\mu s \tag{3.1}$$

The delay oscilloscope was then set so that a signal was sent to trigger the ruby laser after a delay of T_{AB} seconds. The Pockels cell voltage for Pulse #1 of the ruby laser was set to zero, thus eliminating Pulse #1 from the firing sequence.

9
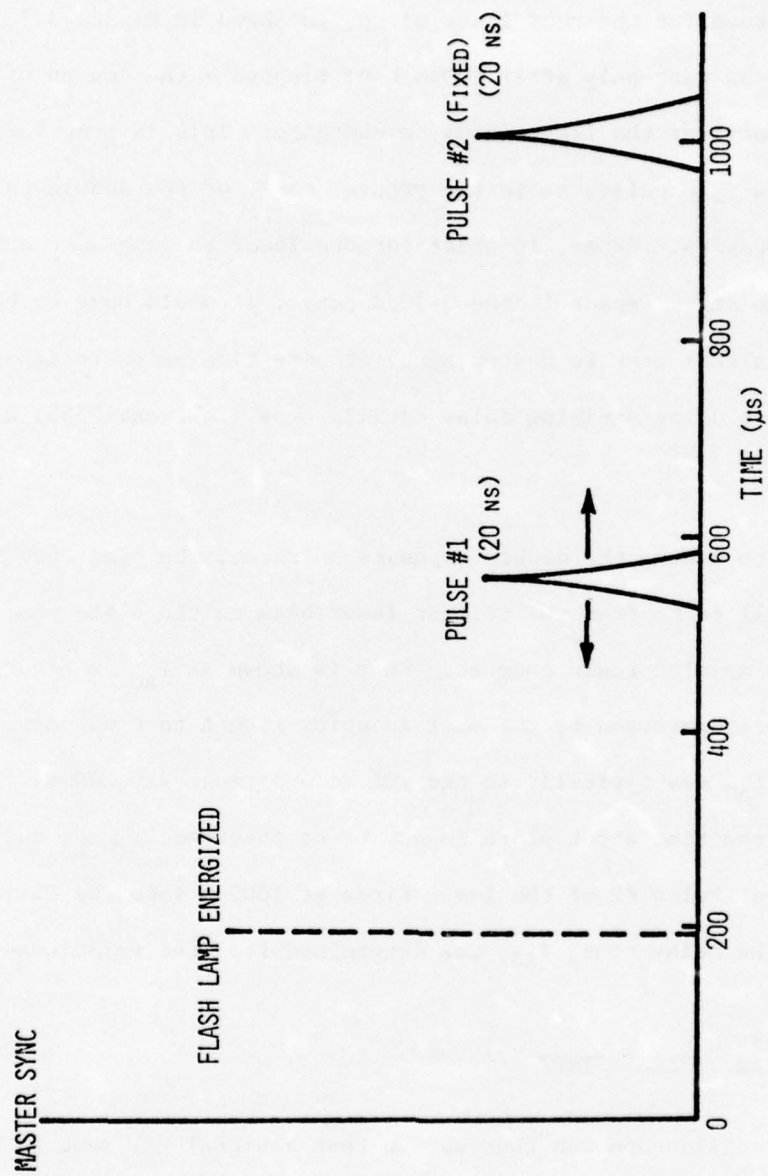
Figure 3.3 - Timing Sequence for Pulsed Ruby Laser
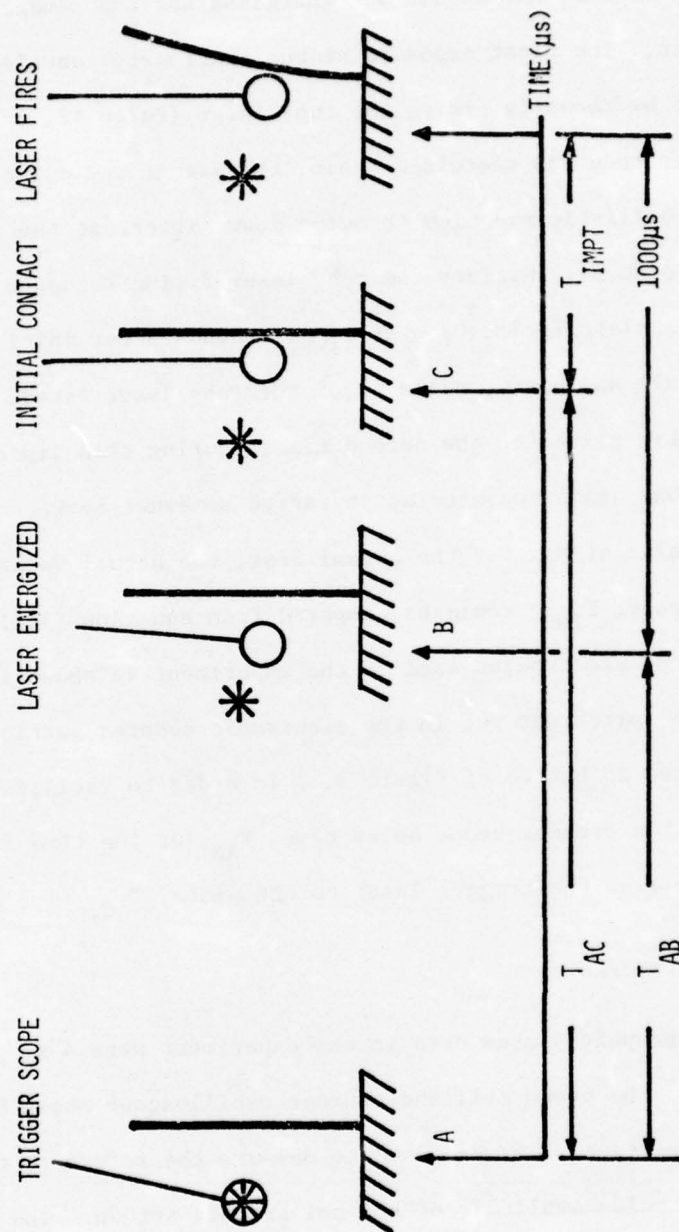
Figure 3.4 - Impact/Laser Timing Sequence

11

With the steps mentioned above carried out, the actual impact test was run. First, the magnet was energized and the pendulum attached to it. The first exposure of the stationary cantilever plate was then made by manually firing the ruby laser (Pulse #2, only). The ruby laser then was energized again, the magnet was switched off, allowing the ballistic pendulum to swing down, interrupt the trigger laser beam (point A), initiate the ruby laser firing sequence (point B), and impact the plate (point C). At T_{IMPT} seconds after initial contact between the ball and plate, Pulse #2 of the ruby laser fired, exposing the photographic plate for the second time. During this impact sequence, the time T_{AC} was again measured as it varied somewhat between tests. Knowing the value of T_{AC} for the actual test, the actual value of the time after impact, T_{IMPT} could be computed from equation (3.1). A schematic of the electronics used in the experiment is shown in Figure 3.5. A switch was put in the electronic counter portion of the circuit (located at bottom of Figure 3.5) in order to facilitate quick monitoring of the present scope delay time, T_{AB}, or the time it took the ball to go from the trigger laser to the plate, T_{AC}.

3.3 Hologram Processing

The photographic plates used in the experiment were 4"x5" Agfa-Gevaert 10E75. The photo cell and storage oscilloscope shown behind the hologram in Figure 3.5 were used to measure the reference to object beam ratio and pulse amplitude of the holographic set up. The beam ratio for the tests was approximately 2 to 1 (reference beam to object beam). The combination of photo cell and storage oscilloscope could only give

12
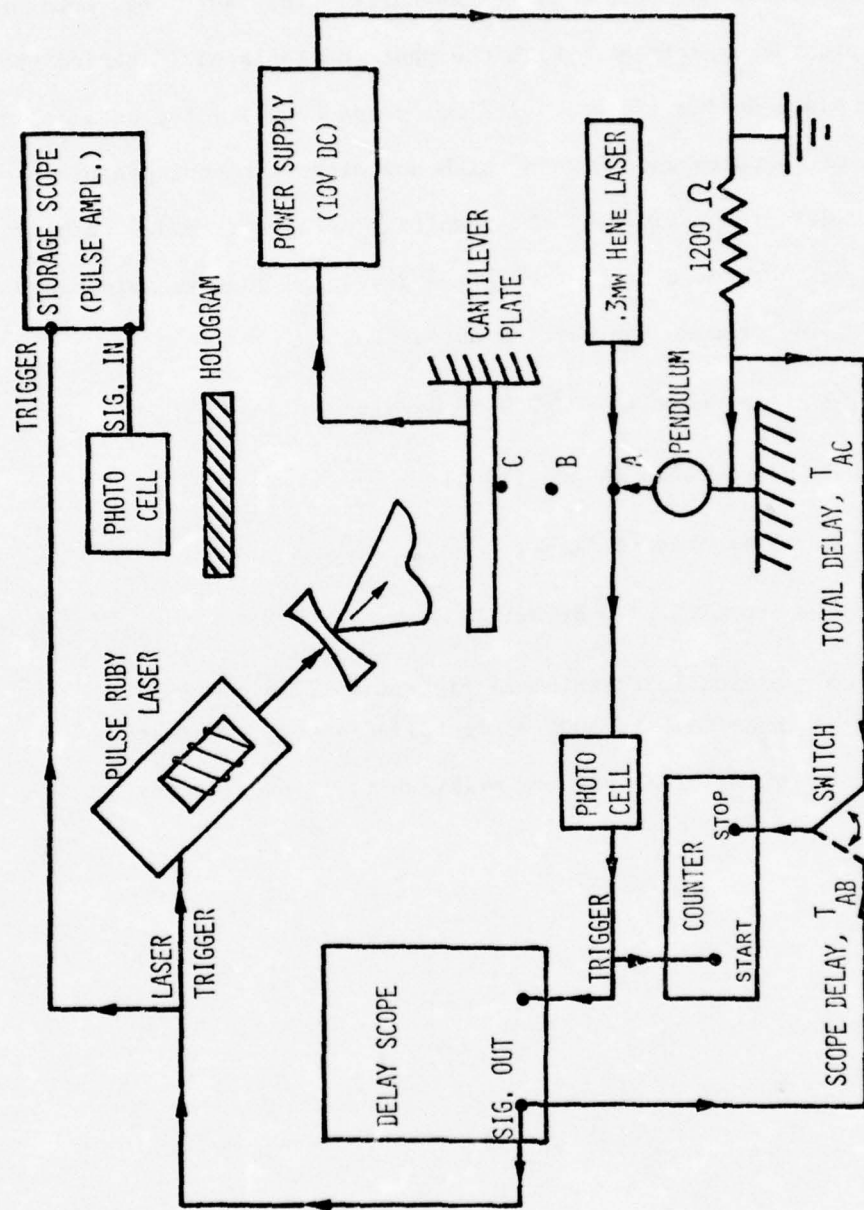
Figure 3.5 - Electronic Circuitry for Making a Double Exposure Hologram

relative light intensity measurements, i.e., the amplitude of the reference beam relative to the object beam or the relative amplitude between the first and second plate exposures. This sufficed, however, for the present experiment. With the photo cell placed 1" behind the hologram plate holder, "acceptable" holograms resulted for oscilloscope readings of .4 volts and .6 volts with and without a photographic plate in the holder, respectively. The resulting holograms tended to be dark but this was corrected by bleaching the developed photographic plates. The developing process was carried out as follows:

1. 4 minutes in Kodak D-19 developer;

2. 30 seconds in stop bath;

3. 3 minutes in fixer;

4. Dry with blow dryer;

5. Bleach in Potasium Ferricynanide (15g of $K_3Fe(CN)_6$ in 1000 ml distilled water) - agitate until plate becomes milky white, approximately 1 minute.

SECTION IV

EXPERIMENTAL DATA REDUCTION AND RESULTS

Figures 4.1 through 4.5 show the cantilevered plate's
response for times after impact ranging from 2μs to 33μs. For the
sake of increased fringe clarity, the photographs taken of the
holograms show the immediate area of impact. Recall that the
impact point lies on the vertical axis of the plate and 3 inches
above the clamped base. The numbers in parentheses refer to the
raw data numbering system used to denote each test run. The
6061-T6 aluminum plate was painted with a flat white paint and
a grid having 1" by .5" increments was scribed on it. In addition,
1/8" increments were scribed on the plate centerline from the
impact point to 1" below it.

Referring to Figures 4.1 through 4.5, the fringes concentrically
located around the impact point (ball impacting from rear) represent
loci of constant displacement on the plate. The fringes are a contour
map of the flexural waves caused by the impact. They travel outward
with time until they reach the free edge of the plate at about T=12μs
and are reflected. It is evident from the photographs that either
the timing measurements are in error by as much as ± 2μs or that there
was some scatter in the magnitude and duration of the impulse load
imparted to the plate by the steel ball pendulum. The latter reason
is thought to be the case because of a permanent magnetic field that

15

6 μs (90)

4 μs (89)
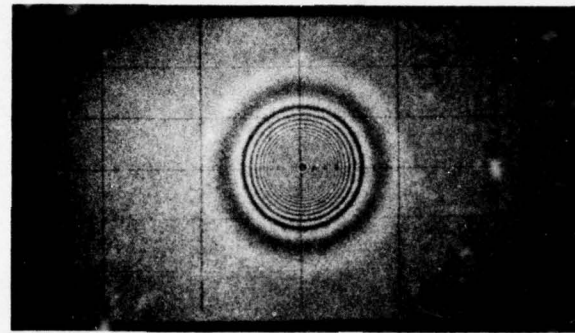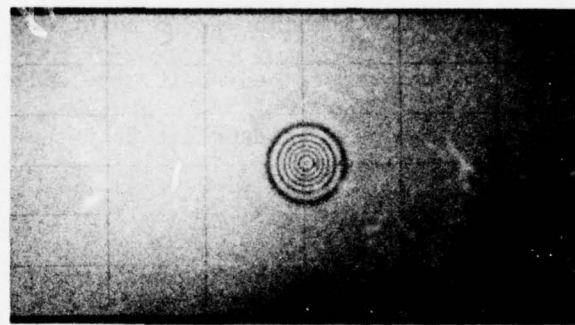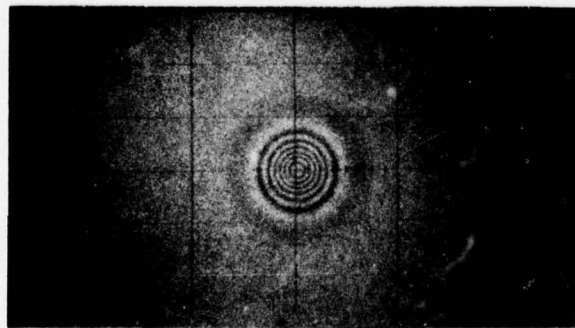
2 μs (91)

Figure 4.1 - Double Exposure Holograms of Cantilever Plate (2, 4, and 6μs)

16

(95) 11 μs

(98) 10 μs

(101) 9 μs
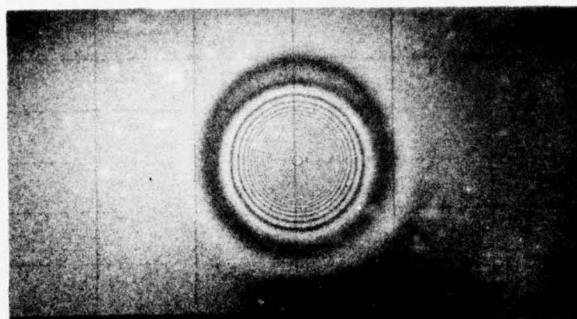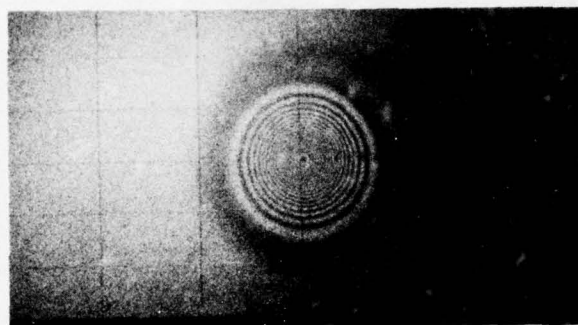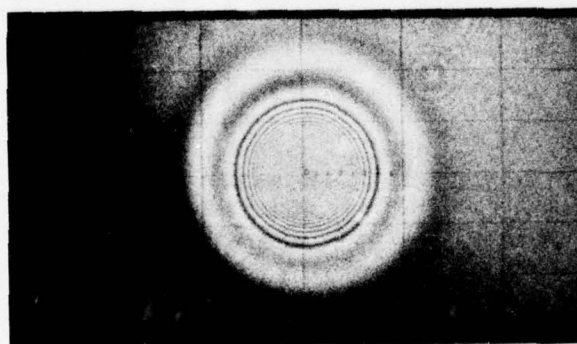
Figure 4.2 - Double Exposure Holograms of Cantilever Plate (9, 10, and 11μs)

17

12 µs   (107)
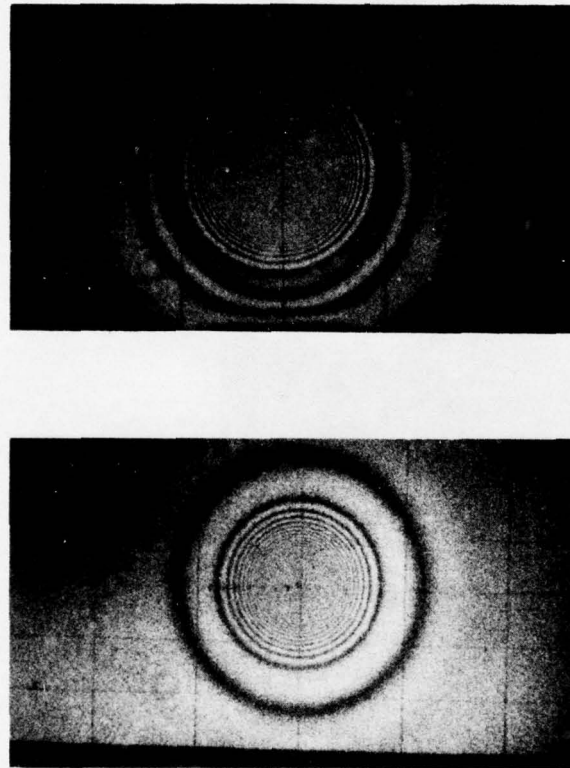
13 µs   (96)

Figure 4.3 - Double Exposure Holograms of Cantilever Plate (12 and 13µs)

18

24 μs   (108)

18 μs   (106)
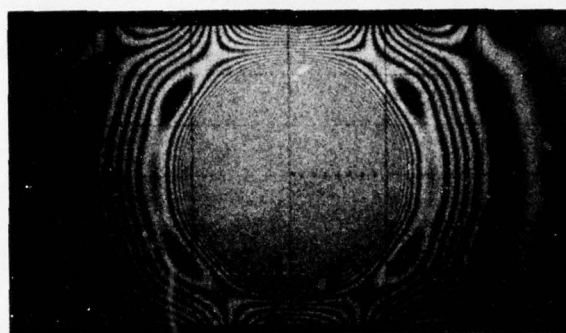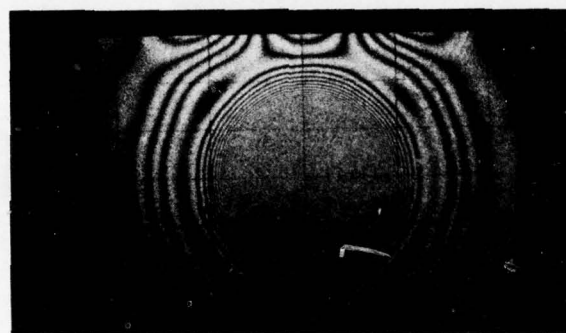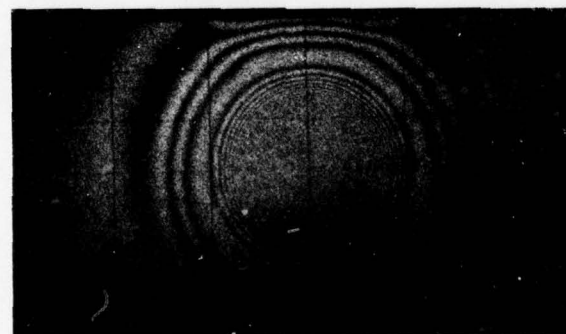
16 μs   (93)

Figure 4.4 - Double Exposure Hologram of Cantilever Plate (16, 18, and 24μs)

19

33 μs   (103)

30 μs   (105)

28 μs   (110)
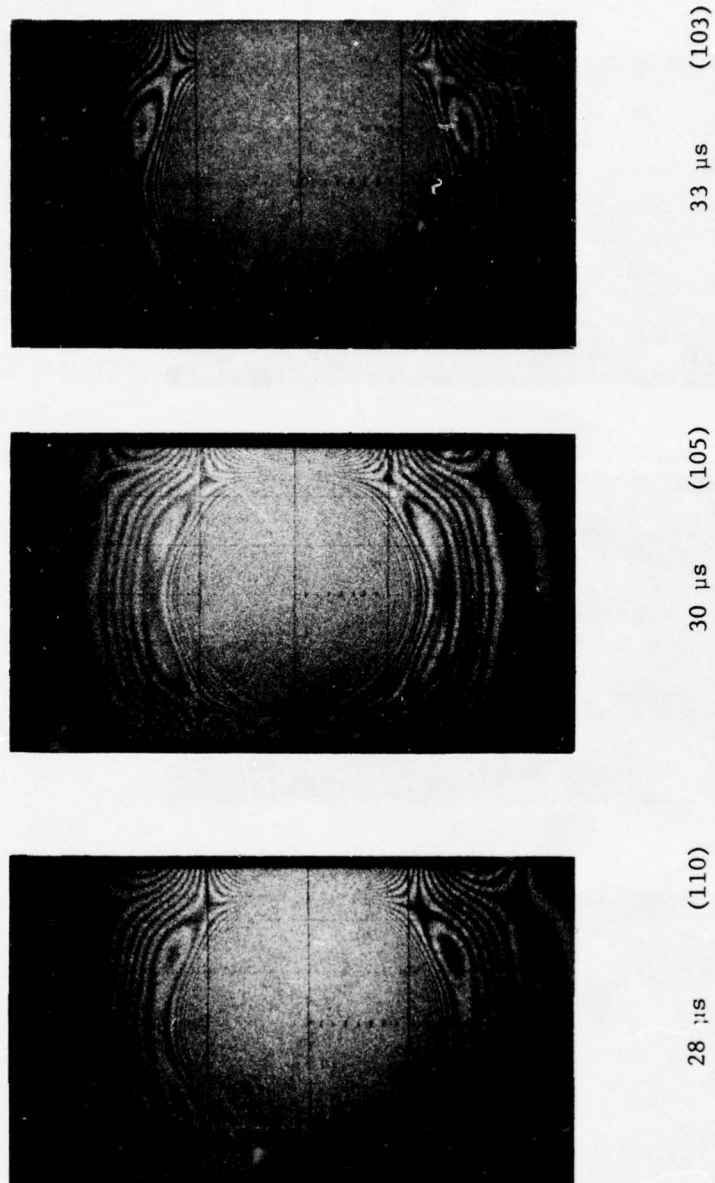
Figure 4.5 - Double Exposure Hologram of Cantilever Plate (28, 30, and 33μs)

20

was induced in the electromagnet used to release the steel ball. The permanent magnetic field varied somewhat throughout the duration of the impact tests. The magnetic force field would have the effect of slowing up the ball's release and, consequently, decreasing its impact force. This fact is corroborated by Figures 4.6 and 4.7 where the force time profile is seen for four successive ball impacts on a pressure transducer (Piezotronics, PCB 118A-B, 2μs rise time) temporarily imbedded in the plate at the impact point. The pressure amplitude (proportional to force) in test 1 is 20% less than the tests 2 through 4. While future work in this area should strive for a more repeatable loading system, the present data scatter was found to be acceptable within the scope of the present research effort. The load profile shown in Figures 4.6 and 4.7 was also utilized to determine the loading input for the finite element analysis (Section 5.1).

The fringe pattern position and the corresponding times after impact in Figures 4.1-4.5 can be used to compute the velocity of the flexural waves in the plate. Using the outermost visible fringe for times after impact ranging from 2μs to 13μs, one can get a plot of wave position as a function of time. The slope of this curve will be the flexural wave velocity. Using the fringe pattern positions and corresponding times in Figures 4.1 through 4.3, the curve shown in Figure 4.8 was generated. Because of the aforementioned scatter due to load repeatability, a linear least squares routine was used to generate the curve through the data points. The slope of the curve gives the flexural wave velocity as $C_f = .1024$ in/μs.
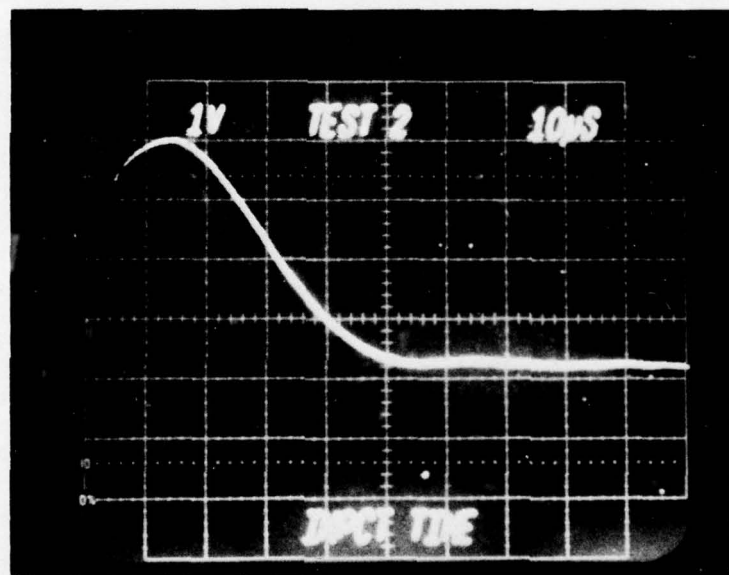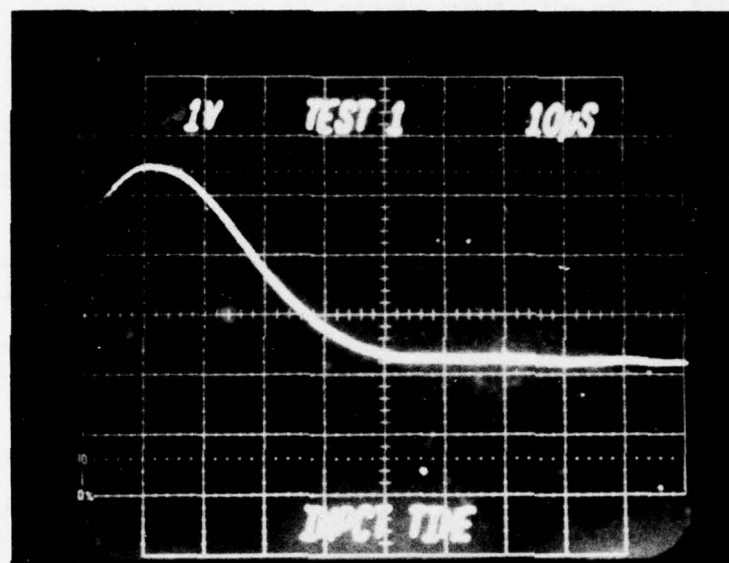
Figure 4.6 - Pressure Transducer Output at Impact Point Vs
Time (Tests 1 and 2)
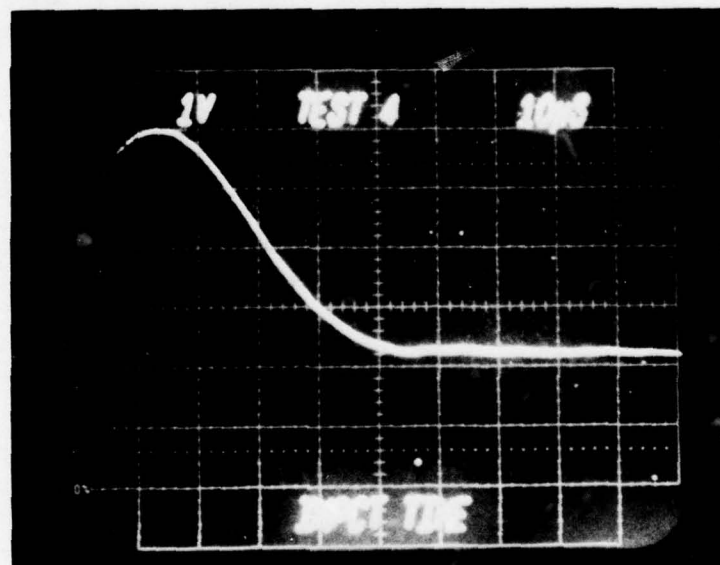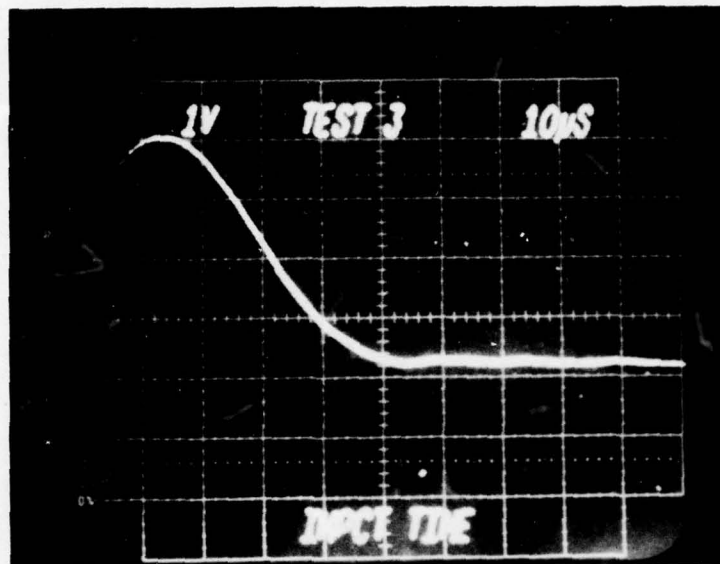
Figure 4.7 - Pressure Transducer Output at Impact Point
Vs Time (Tests 3 and 4)
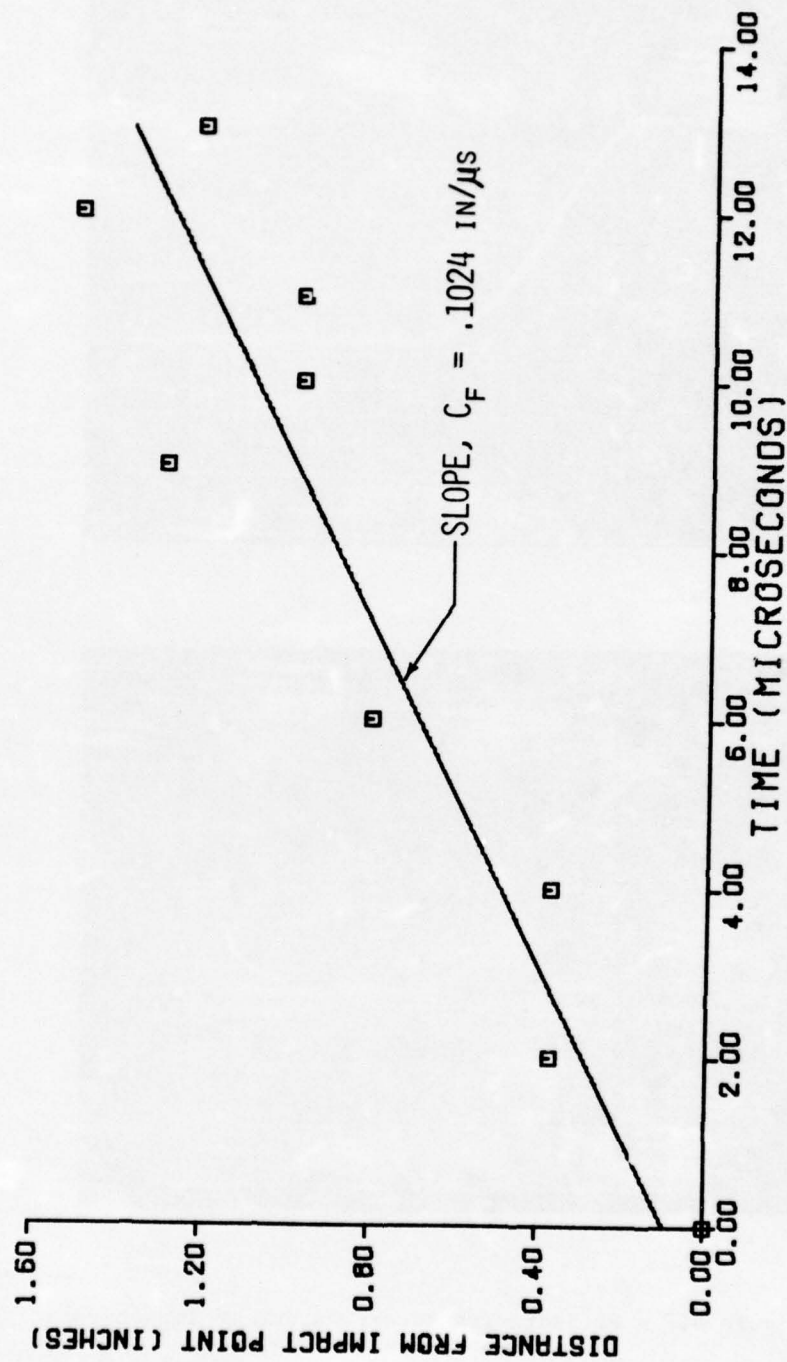
Figure 4.8 - Flexural Wave Position As a Function of Time After Impact

24

It is of interest to compare the experimental value of the
flexural wave velocity to that obtained using the three-dimensional
equations of elasticity (Ref. 2, 3, and 4). According to classical
plate theory, the flexural wave velocity in an infinite plate approaches
that of a Rayleigh surface wave when the wavelength, λ, becomes small
compared with the plate thickness, h. In the case of the present
impact tests, the steel ball made contact with the plate over a
circular area of less than .03125 inches in diameter. Now, the wave-
length, λ, is a function of the pulse shape and plate contact area,
and if the pulse loading is broken into its Fourier components, the
largest component's wavelength will be on the order of twice the
diameter of the contact area. Hence, the smallest value of h/λ for
the plate with h = .1875 is h/λ = 3. All other values of h/λ for the
higher Fourier components will be greater than this value. For values
of $h/\lambda > 3$, the flexural wave velocity in a plate closely approximates
that of a Rayleigh surface wave and can be obtained from the expression
(Ref. 4).

$$C_f = .932 \; C_s \qquad (\nu = 1/3) \qquad\qquad (4.1)$$

where $C_s = \sqrt{\dfrac{G}{\rho}} = \sqrt{\dfrac{E}{2(1+\nu)\rho}}$ is the shear wave velocity.

For the test plate; $E = 1 \times 10^7$ psi, $\nu = .3$, and
$\rho = 2.587 \times 10^{-4}$ lbm. Placing these values into equation (4.1)
yields a value of $C_f = .112$ in/μs. This is within $\pm 8.5\%$ of the
experimental value.

25

The magnitude of the plate's displacement can be obtained from the fringe photographs using the expression (Ref. 5 and 6):

$$\vec{\delta} \cdot (\vec{n}_o + \vec{n}_v) = \frac{(2N \mp 1)\lambda}{2}, \quad \text{for} \quad N = \pm 1, \pm 2, \pm 3 \ldots \quad (4.2)$$

where $\vec{\delta}$ - displacement vector

$\vec{n}_o$ - unit vector in direction from object to illumination source (object beam)

$\vec{n}_v$ - unit vector in direction from viewer (through hologram) to object

λ - wavelength of laser used to make the hologram

N - fringe order

The vectors given by equation (4.2) are shown in the context of the present experimental geometry in Figure 4.9.

Carrying out the dot product in equation (4.2) yields:

$$|\vec{\delta}| |\vec{n}_o + \vec{n}_v| \cos(\vec{n}_o, \vec{n}_v) = \frac{(2N \mp 1)\lambda}{2} \quad (4.3)$$

letting $|\vec{\delta}| \equiv \delta$ and using Figure 4.9 gives

$$|\vec{n}_o + \vec{n}_v| = |1.975 \vec{i} + .222 \vec{j}| = 1.987 \quad (4.4)$$

$$\cos(\vec{n}_o, \vec{n}_v) = .975 \quad (4.5)$$

26
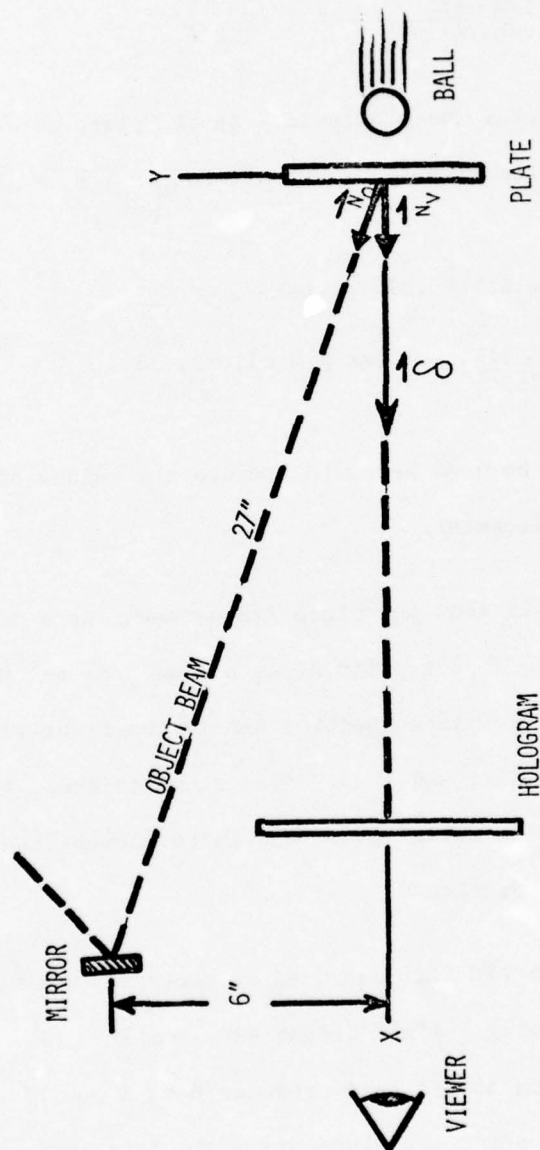
Figure 4.9 - Vector Diagram For Normal Displacement Computation

27

Hence, the displacement, δ, in the direction that bisects $\vec{n}_o$ and $\vec{n}_V$ is:

$$\delta = \frac{(2N \mp 1)\lambda}{(2)(.975)(1.987)} = \frac{(2N \mp 1)\lambda}{3.874} \tag{4.6}$$

The displacement normal (perpendicular) to the plate surface differs from that given in equation (4.5) by only $\text{Cos}\left(\dfrac{\vec{n}_o, \vec{n}_V}{2}\right) = .994$.

Dividing equation (4.6) by .994 gives

$$\delta_n = \frac{(2N \mp 1)\lambda}{3.853}, \qquad \text{for } N = \pm 1, \pm 2, \pm 3 \ldots \tag{4.7}$$

Equation (4.7) will be used below to compute the values of the plate's normal displacement.

Figures 4.10-4.13 show the plate displacement as a function of the distance from the impact point along a line from the impact point to the free edge of the plate (Section A-A in the figures) for times after impact of 4, 6, 12, and 18µs. Also shown in these figures are the normal displacement curves based on finite element analysis which will be discussed in Section V.

Polaroid type 55 P/N film was used to photograph the double exposure holograms using a 4"x5" format view camera with a Polaroid film holder. Polaroid 55 P/N film produces both a positive and negative print. The negative print was placed in a standard photographic enlarger such that the enlarged view of the displacement fringes could be used to more accurately determine the corresponding displacement. Using the enlarger, fringes as high as N=70 could be
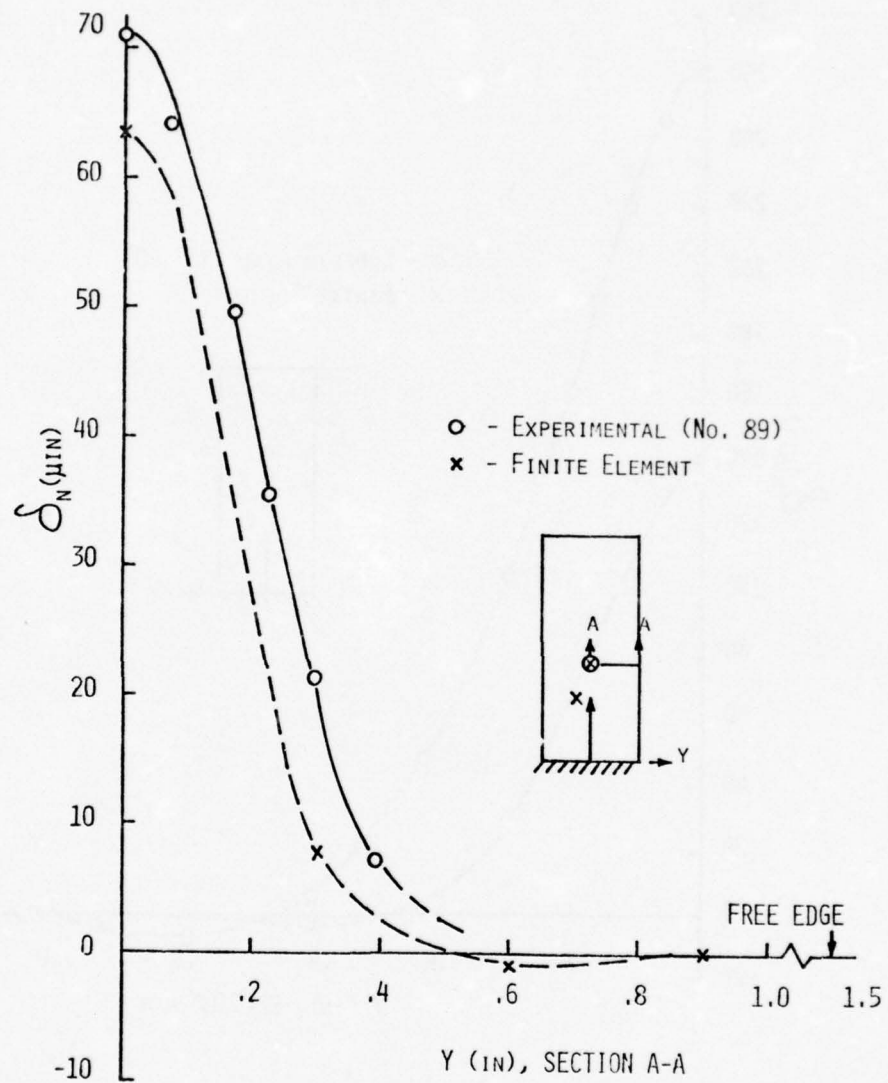
Figure 4.10 - Normal Displacement, δ_n, Vs Distance From
Impact Point, Y, at $T=4\mu s$

29
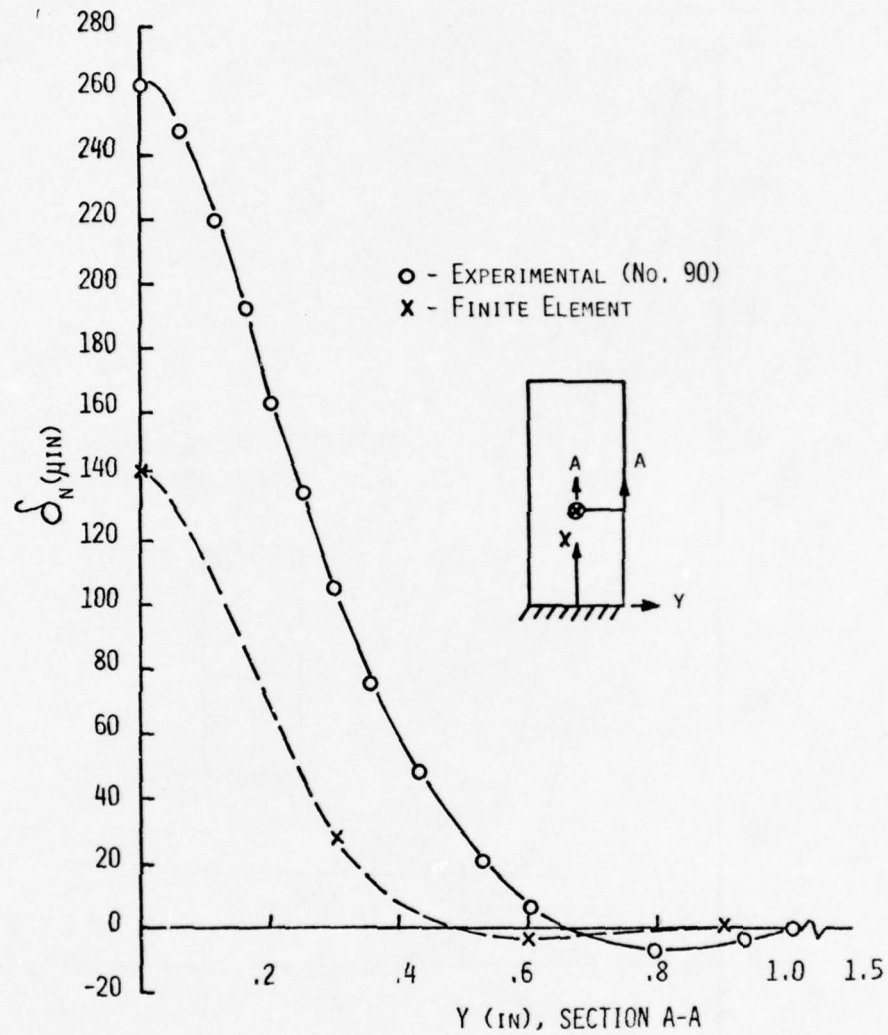
Figure 4.11 - Normal Displacement, δ_n, Vs Distance From

Impact Point, Y, at T=6us
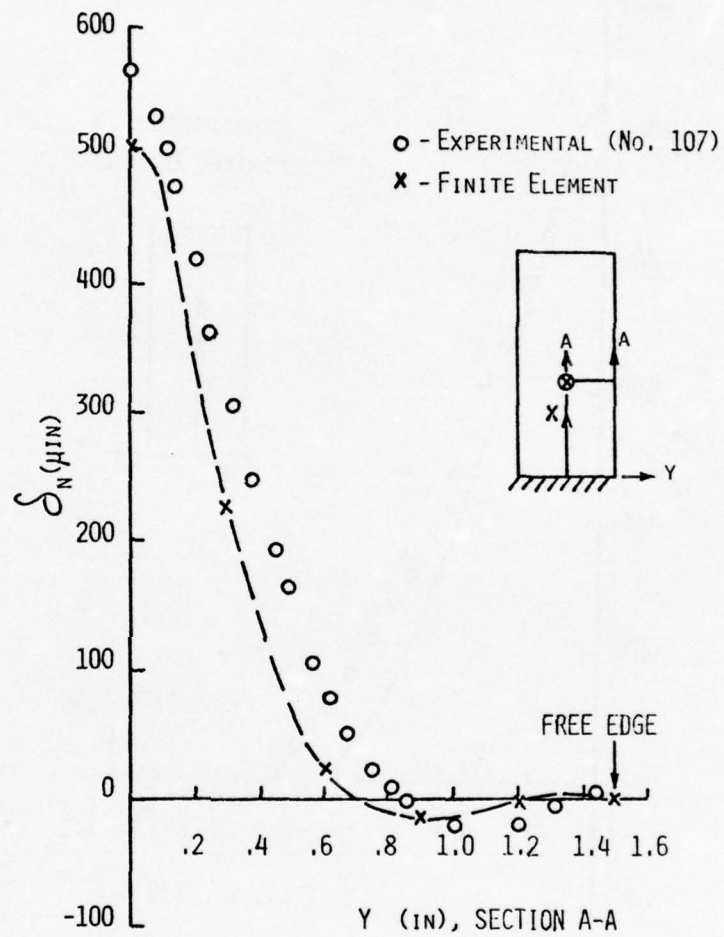
Figure 4.12 - Normal Displacement, δ_n, Vs Distance From
Impact Point, Y, at T=12μs
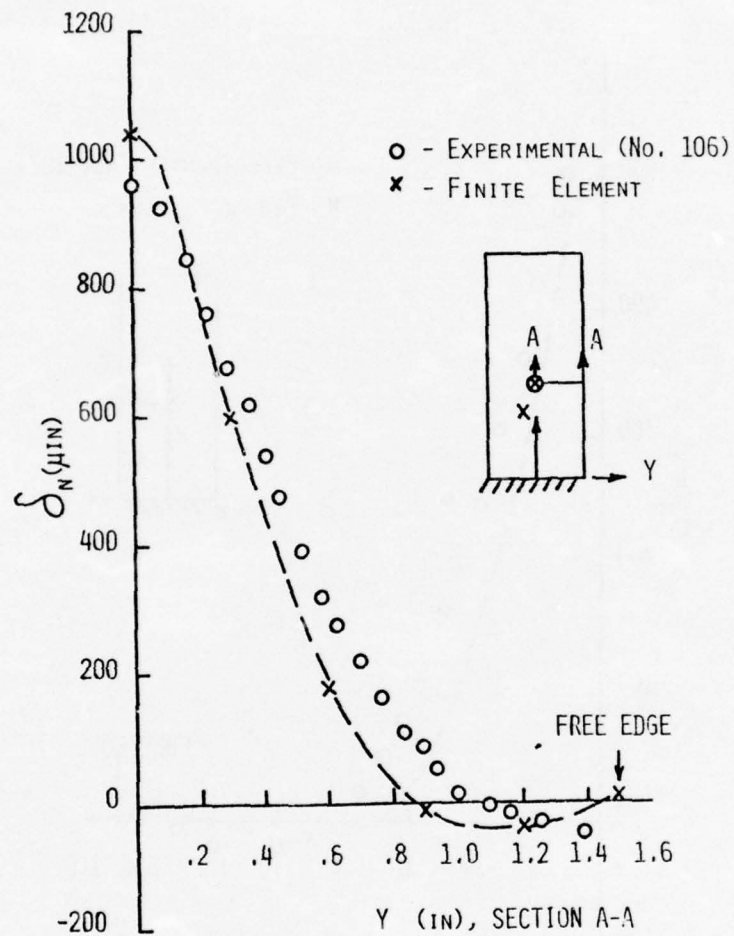
Figure 4.13 - Normal Displacement, δ_n, Vs Distance From

Point, Y, at T=18μs

observed. (Note that this technique could be conveniently expanded to include a digital X-Y plotting table as the projecting surface for the enlarger.)

In contrast to time-average holography where the white fringe denoting zero displacement is the most intense and stands out clearly, the fringe representing zero displacement in double exposure holography is of the same intensity as its neighboring higher order fringes. Hence, in order to get a quantitative plot of the displacement based on a single hologram, some a priori information on the plate's displacement response is necessary. Referring to Figures 4.1, 4.2, and 4.3, the maximum plate displacement occurs at the impact point and decreases in magnitude as one travels outward from it. Since the flexural displacement is a wave, the positive displacement at the impact point will be followed by a smaller negative one at some distance from the impact point and then, as one travels further away from the impact center, a return to the undeformed, zero displacement, portion of the plate. The peak negative displacement manifests itself by a widening of the fringes where the slope of the negative displacement goes to zero. This can be seen in Figure 4.3 in the 12µs (107) photograph. Using this type of reasoning the plate's normal displacement could be plotted. While this approach was found to be sufficient for the simple deformation pattern that the plate experienced, more complex displacements would necessitate more sophisticated approaches such as multiple double exposure holograms. As an aside, another approach that could be used to determine the zero displacement fringe would be to use an optical bench telescope

33

to scan across the image of the hologram. By scanning along a
horizontal line passing through the impact point, the concen-
trically located fringes will appear to converge toward one of
the circular fringes. In other words, the impact point will
appear to be a fringe "source" with fringes traveling toward
the one stationary circular fringe. Fringes located outside
the stationary circular fringe will appear to travel in the
direction of the impact point and the stationary circular fringe.
The stationary fringe is a loci of zero displacement and by
viewing the convergence (traveling) characteristics of the
adjacent fringes, it can be located.

Figure 4.14 shows a plot of the plate's normal displacement
along its free edge (Section B-B) at T=24μs after impact. The
displacement curve is based on the third fringe photograph shown
in Figure 4.14 and shown enlarged in Figure 4.15. The fringes
are numbered in Figure 4.15. Along the free edge, the undeformed
plate was used as the zero reference point. In addition, fringes
that curved from one point on the free edge to another provided a
convenient indicator of points of equal displacement on the
opposite sides of a hill or a valley.
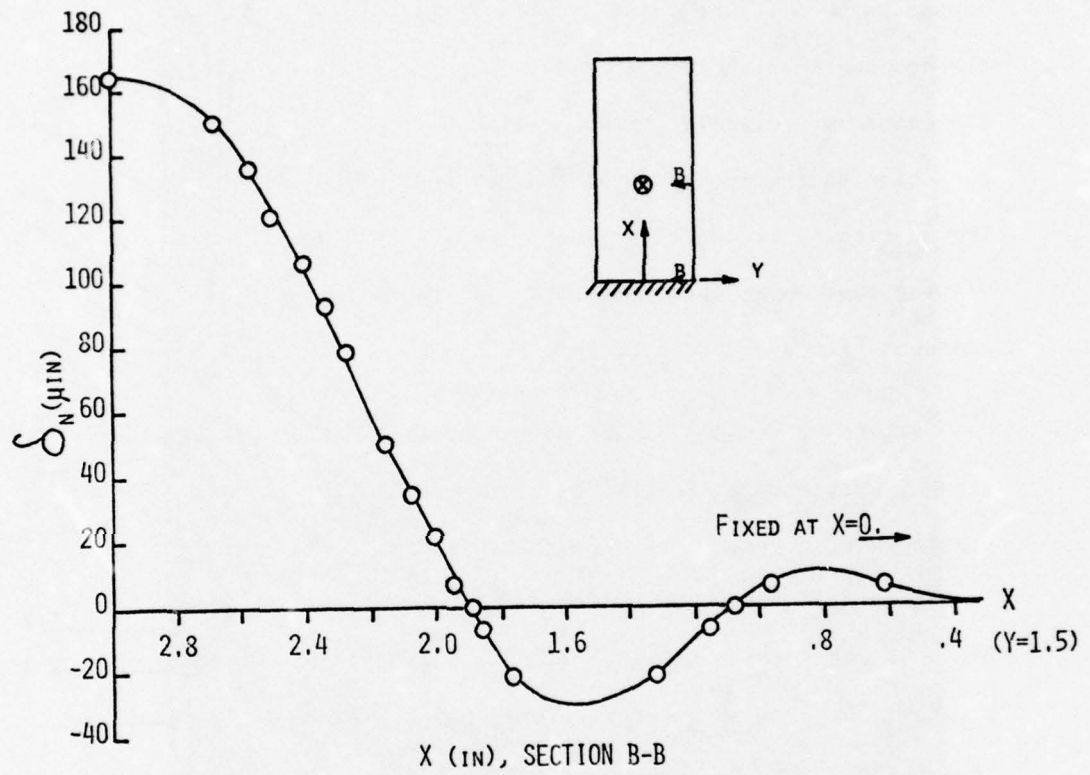
Figure 4.14 - Normal Displacement Along Plate Free Edge
at T=24μs
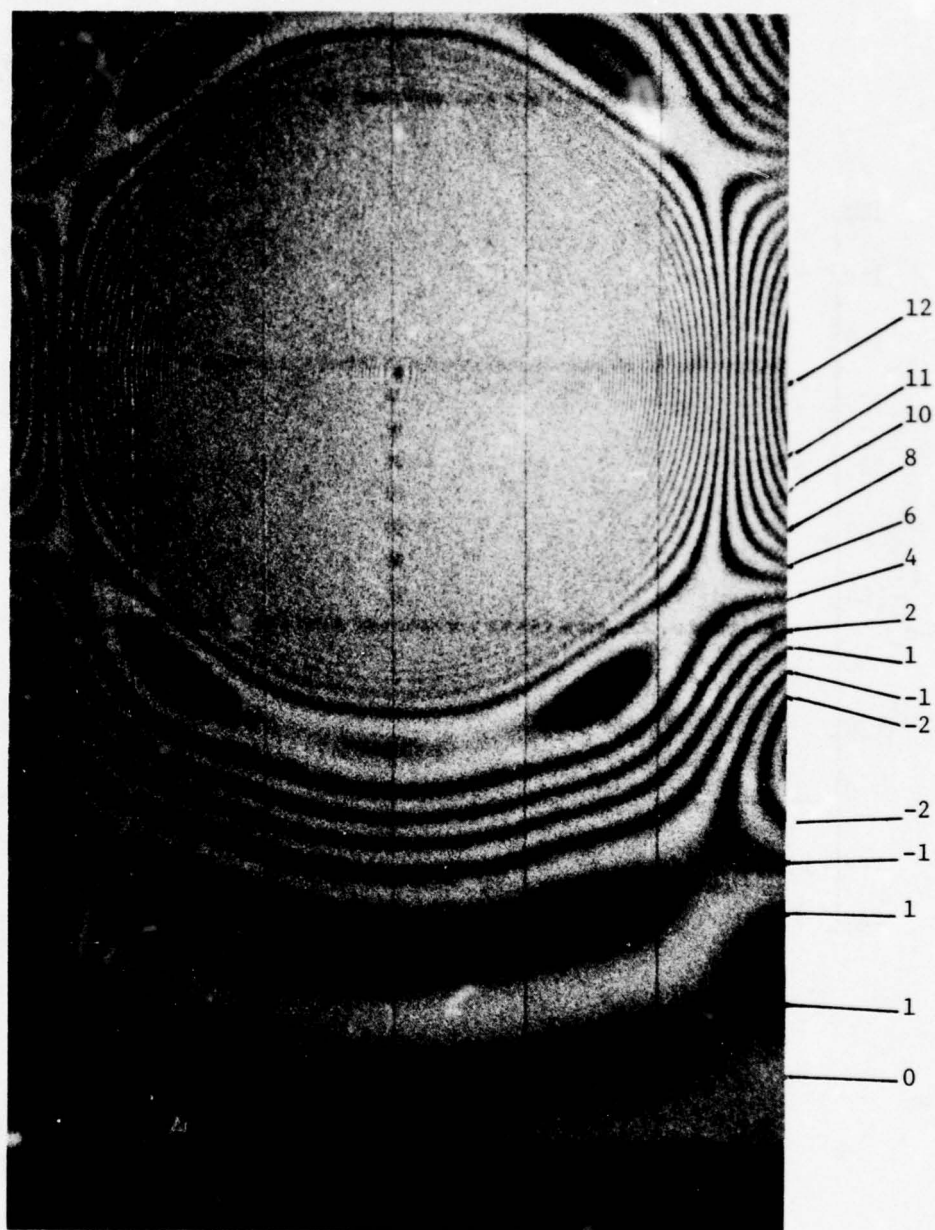
Figure 4.15 - Enlarged View of Impacted Plate at T=24μs Showing
Numbered Fringes

SECTION V

FINITE ELEMENT ANALYSIS AND RESULTS

5.1 Finite Element Model

The numerical portion of the study was based on a finite element analysis of the cantilever plate using the general purpose finite element computer program, NASTRAN (Navy Nastran, Level 15.2.0). The model geometry and orientation for the cantilever plate is shown in Figure 5.1. The mesh consists of 304 nodes that connect the 165 quadrilateral plate elements (CQUAD2). The nodes at the base of the plate were fixed against both translation and rotation to simulate the cantilever condition. Because the impact load acts symmetrically with respect to the long axis of the plate, only half the plate was modelled with the nodes along the plate's axis of symmetry being fixed against asymmetrical motions, namely, translation in the Y direction and rotation about the X axis. These assumptions yield a finite element model having 957 degrees of freedom. Note that a refined mesh was used in the area about the impact point (shown by arrow). The plate response was essentially the same whether or not the refined mesh was used (thus demonstrating convergence) but better contour plots resulted when the finer mesh was used.

The transient analysis module of NASTRAN, Rigid Format 9, was used to carry out the analysis. When using the transient analysis module one can elect to use either a modal superposition technique or a direct integration of the nodal displacements. The latter

37
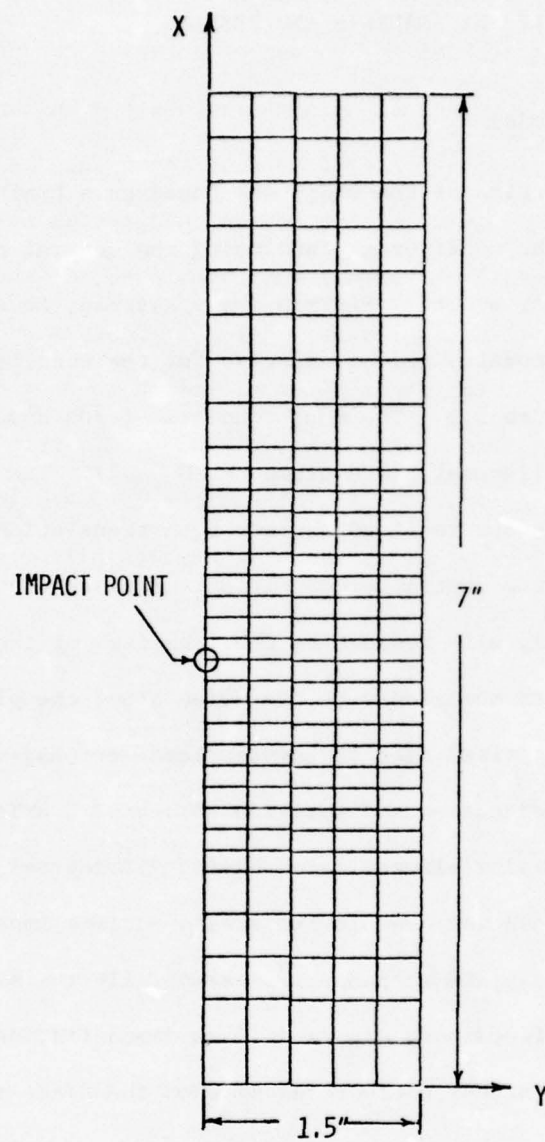
Figure 5.1 - Finite Element Mesh of Cantilever Plate

technique of direct integration was adopted for this study because it would have taken a prohibitive number of normal modes and frequencies to effectively model the plate response for an impact load that had a duration of 55µs. A good rule of thumb when using the modal superposition method is that both the integration step size and the period of the highest normal mode should be, at most, one-tenth the size of the force duration. For the present study, this would have required the highest mode of vibration to have a period of about 5µs, i.e., a natural frequency of 2×10^5 Hz. This fact, coupled with the additional fact that the direct integration technique is inherently more accurate since it handles all degrees of freedom, lead to its choice as the solution technique.

The transient analysis module of NASTRAN accepts the forcing function in tabular form where the load amplitude and direction versus time are input for each node in the area of the load. For the present study, a single load in the normal (Z) direction was input as a function of time at the node designated by the arrow in Figure 5.1 (node number 171). The load profile was assumed to be the shape of a half sine wave (see Figures 4.6 and 4.7) having a duration of 55µs. By measuring the height of the ballistic pendulum at its release point and at its maximum rebound position from the plate, the amplitude of the half sine load can be obtained by equating the maximum kinetic energy to the maximum potential energy of the pendulum. For a pendulum of mass, m, being released at height, h_1, and rebounding to a height of h_2, equating the maximum potential and kinetic energies

39

AFAPL-TR-76-56

yields a change in velocity of:

$$V_1 - V_2 = \sqrt{2g} \quad (\sqrt{h_1} - \sqrt{h_2}) \tag{5.1}$$

where g is the acceleration of gravity.

The impulse of the force, F(t), acting

for a time, T, is

$$I = \int_0^T F(t)dt = m (V_1 - V_2). \tag{5.2}$$

For a force having a half sine wave profile,

$$F(t) = A \sin \left(\frac{\pi t}{T}\right) \tag{5.3}$$

where A is the force amplitude.

Utilizing equations (5.1) and (5.3) in equation (5.2) yields

$$I = \int_0^T A \sin \frac{\pi t}{T} dt = m \sqrt{2g} \quad (\sqrt{h_1} - \sqrt{h_2}) \tag{5.4}$$

Carrying out the integration and solving for

the amplitude gives:

$$A = \frac{\pi m \sqrt{2g} \quad (\sqrt{h_1} - \sqrt{h_2})}{2T} \tag{5.5}$$

The mass of the steel ball was 1.335×10^{-3} slugs. From

Figure 3.1, it is seen that $h_1 = 9.75''$. The rebound height was

measured by taking a photograph of the ball's trajectory while

illuminating it with a high frequency strobe light. The height, h_2,

was found to be .263". Placing these values into equation (5.5)

yields an amplitude of A = 230 lbf. Hence, the force on the
plate is

$$F(t) = 230 \sin \left(\frac{\pi t}{55 \mu s} \right) \tag{5.6}$$

Equation (5.6) was used in tabular form in NASTRAN. (This is
done using the "DAREA" and "TABLED1 75" bulk data cards in NASTRAN
as shown in the Appendix).

5.2 Results of the Finite Element Analysis

Using the finite element mesh, boundary conditions, and impact
load profile described above, NASTRAN computed the plate displacement
for specified times after impact. The output was in the form of dis-
placements at specified nodes plus contour plots of the displacement
for the entire plate. The normal plate displacement was plotted as a
function of the distance (v) from the impact point at X=3" for times
after impact of 4, 6, 12, and 18μs. For purposes of comparison with
the experimental results, the four plots are shown in Figures 4.10
through 4.13 of Section IV as the dashed curves. The agreement
between the experimental and finite element result is quite good
except for T=6μs. This is felt to be due to a stronger than average
impact load for the experimental curve. This agreement is corroborated
by a look at Figure 5.2 where the displacement of the plate impact
point is shown plotted as a function of time. A computer generated
second order least squares curve fit the finite element data exactly,
demonstrating a parabolic relationship between the impact point dis-

41
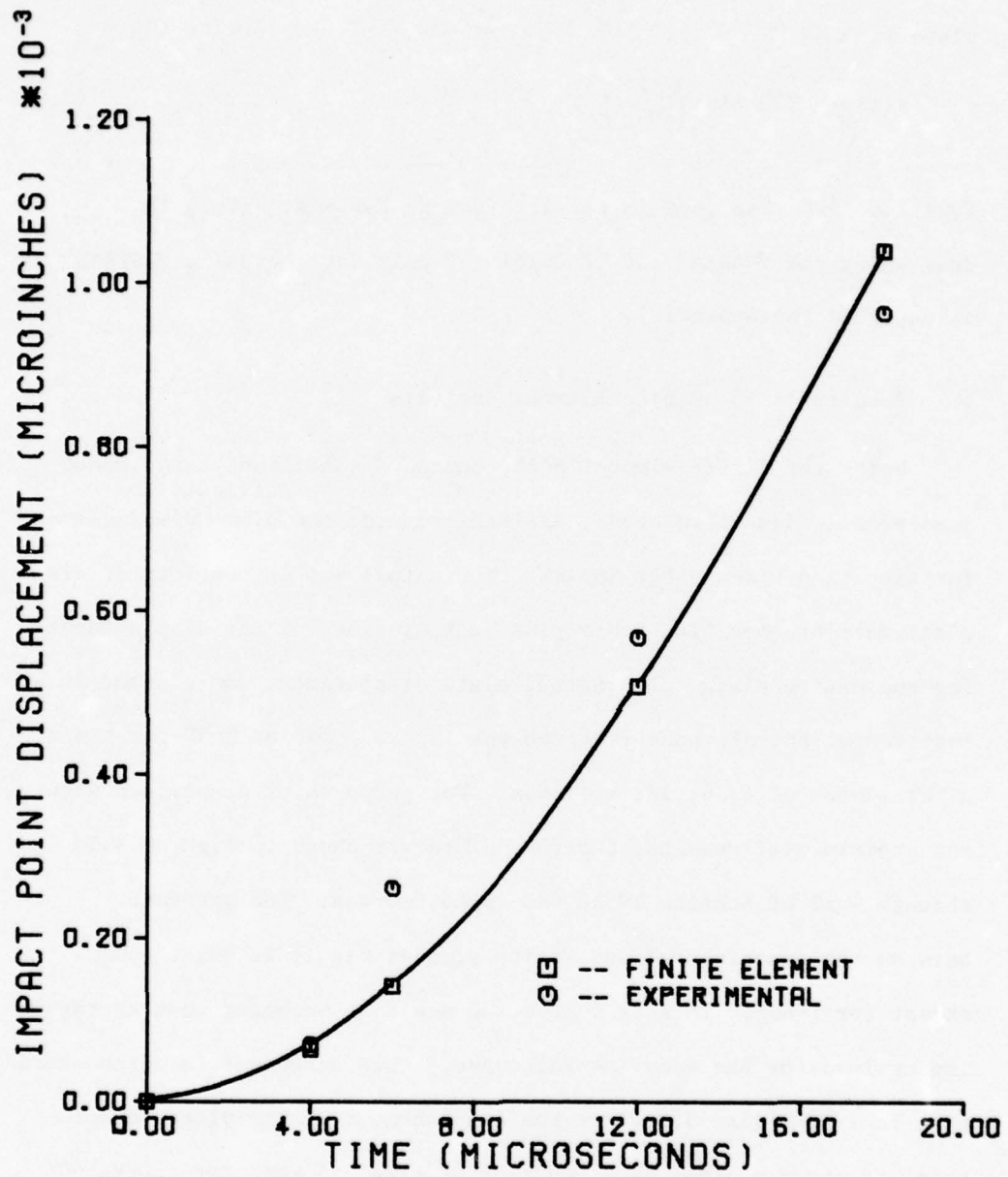
Figure 5.2 - Impact Point Displacement Vs Time

placement and time. The experimentally derived points closely follow this curve with the displacement at T=6μs showing the largest deviation, as one would expect.

Figures 5.3 through 5.5 show normal displacement contours of the plate response at times after impact of 6, 8, 12, 18, 24, and 30μs. The values of the contours are given in Table 5.1. The trends demonstrated by the contour plots are in good agreement with the experimental results. Note in Figure 5.5 that reflection has started to take place off the free edge for T=30μs. While some of the symbols in the contour plots may be difficult to discern, the reader can be aided by the fact that contour numbers 1 through 29 represent increasing positive displacement and numbers 30 through 50 represent increasing negative displacement. This means that a loci of zero displacement lies between contours 1 and 31, exclusive.

TABLE 5.1

Normal Displacement Magnitude for NASTRAN Contour Plots (See
Figures 5.3 - 5.5)

SYMBOL	DISPLACEMENT (IN.)	SYMBOL	DISPLACEMENT (IN.)
1	1.00E-05	26	9.00E-04
2	2.00E-05	27	9.50E-04
3	3.00E-05	28	1.00E-03
4	4.00E-05	29	1.05E-03
5	5.00E-05	30	-1.00E-05
6	6.00E-05	31	-2.00E-05
7	7.00E-05	32	-3.00E-05
8	8.00E-05	33	-4.00E-05
9	9.00E-05	34	-5.00E-05
10	1.00E-04	35	-6.00E-05
11	1.50E-04	36	-7.00E-05
12	2.00E-04	37	-8.00E-05
13	2.50E-04	38	-9.00E-05
14	3.00E-04	39	-1.00E-04
15	3.50E-04	40	-1.50E-04
16	4.00E-04	41	-2.00E-04
17	4.50E-04	42	-2.50E-04
18	5.00E-04	43	-3.00E-04
19	5.50E-04	44	-3.50E-04
20	6.00E-04	45	-4.00E-04
21	6.50E-04	46	-4.50E-04
22	7.00E-04	47	-5.00E-04
23	7.50E-04	48	-5.50E-04
24	8.00F-04	49	-6.00E-04
25	8.50E-04	50	-6.50E-04
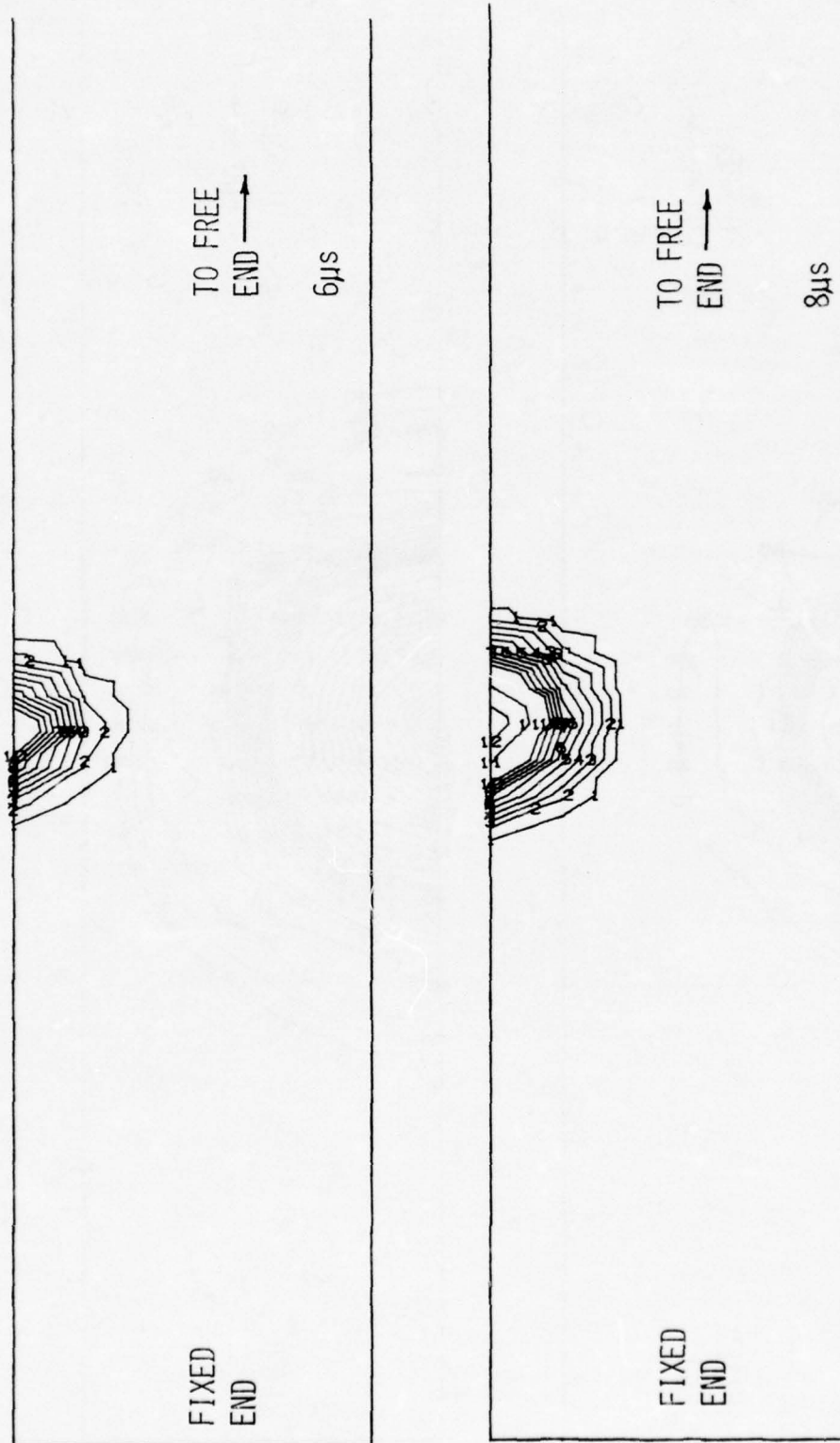
Figure 5.3 - NASTRAN Contour Plot of Normal Displacement at T=6μs and T=8μs
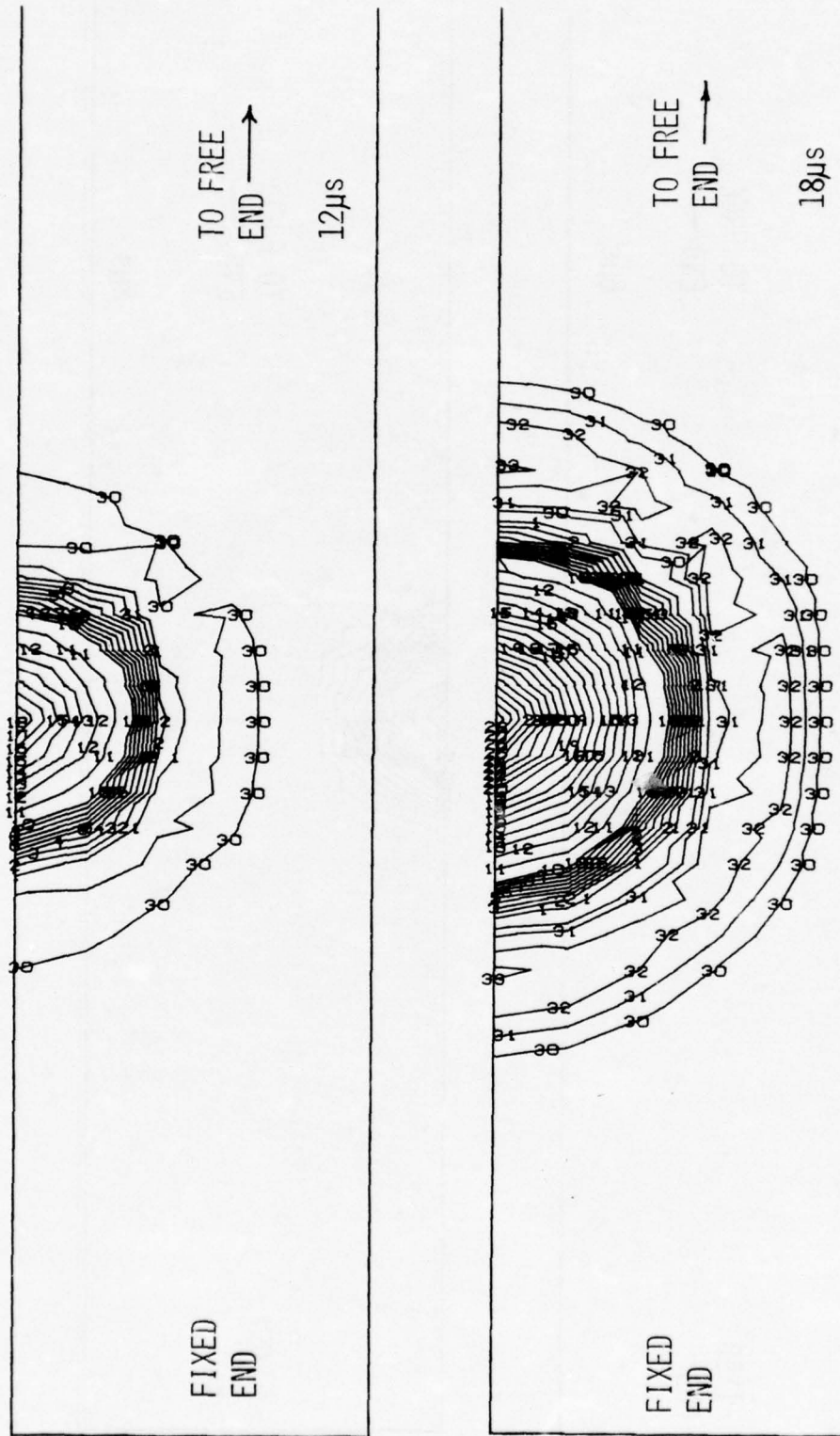
Figure 5.4 - NASTRAN Contour Plot of Normal Displacement at T=12µs and T=18µs
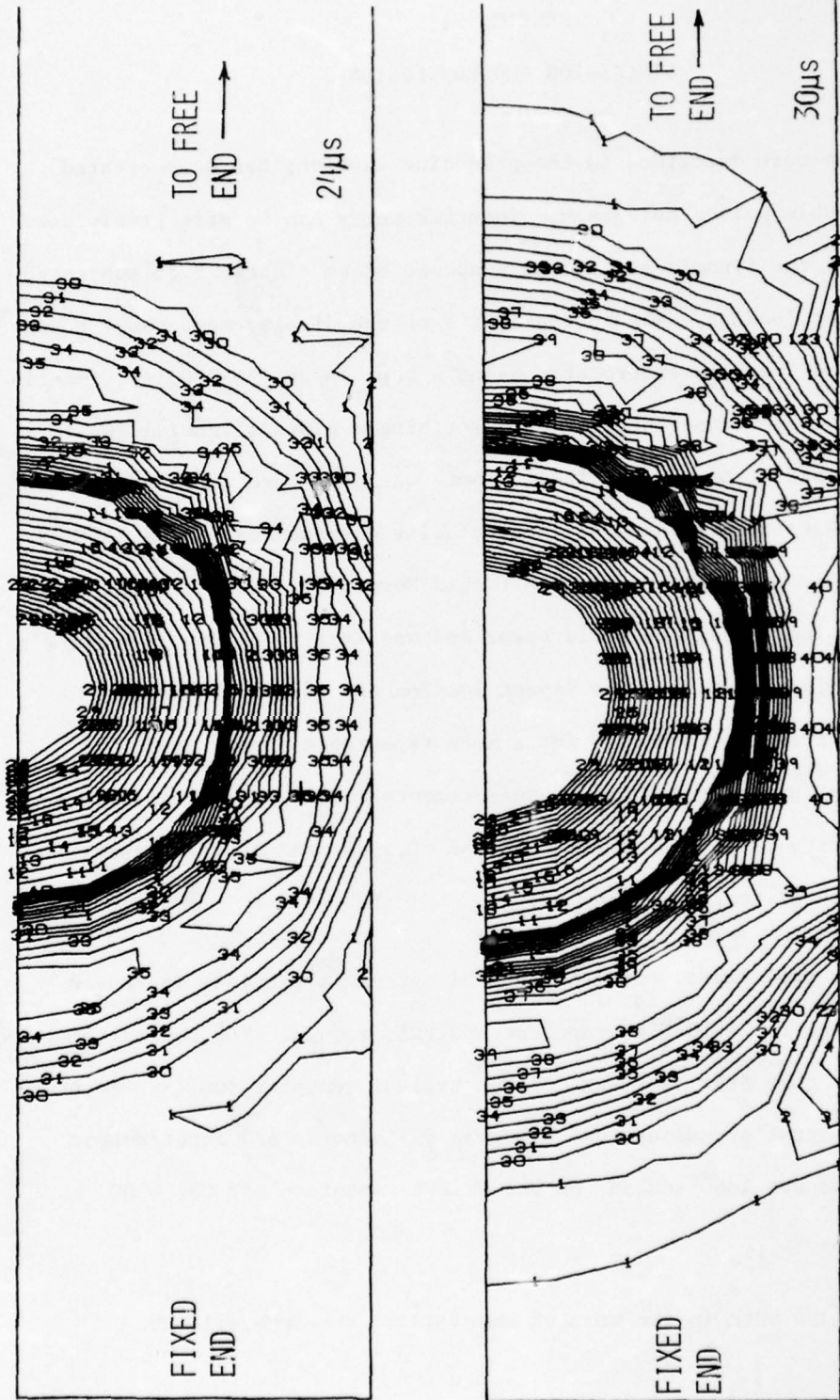
Figure 5.5 - NASTRAN Contour Plot of Normal Displacement at T=24μs and T=30μs

SECTION VI

DISCUSSION AND CONCLUSION

The work described in the preceding sections has demonstrated
that double pulsed holographic interferometry can be effectively used
to study the dynamic structural response of an elastic body subjected
to impact loading. Within the limits of the displacement range covered
by pulsed laser interferometry using a ruby laser (5-1000μin), quanti-
tative displacement information describing a plate's initial response
to an impact load was obtained. There was good agreement between the
experimental tests and analytical results obtained using the NASTRAN
finite element computer program (Rigid Format 9). Some scatter
between individual tests did occur and was felt to be due to failure to
accurately reproduce the impact load on the plate. Future work
in this area should strive for a more repeatable impact load. In
addition, experimental timing measurements should be increased to a
sensitivity of ±0.1 μs instead of the ±0.5 μs used in the present
experimental tests.

The good experimental/analytical agreement provides increased
confidence in NASTRAN's transient analysis module. The good agreement
does not come free, however. For a typical computer run (see Appen-
dix), central processor (CP) time was 923 seconds and input/output
(IO) time was 1360 seconds on the Wright-Patterson AFB CDC 6600
Computer.

Future work in the vein of the current research will use

the existing system to study turbine fan blade response to impact load. Some thought is also being given to utilizing the measurement of the plate flexural wave speed to determine elastic material properties of composites (say) and, also, to study material damping characteristics. Finally, plate displacements, at times greater than those dealt with in this report (2-30μs), could be studied using the double-pulse capability of AFAPL's ruby laser.

REFERENCES

1. Collier, R.J., Burckhardt, C.B.; and Lin, L.H.;
    Optical Holography, Academic Press, New York, 1971.

2. Lamb, H., "On Waves in an Elastic Plate", Proceedings of the
    Royal Society of London, England, Series A, Vol. 93, 1917,
    pp 114-128.

3. Kolsky, H., Stress Waves in Solids, Dover Publications, Inc.
    New York, 1963, pp 16-23.

4. Mindlin, R.D., "Influence of Rotatory Inertia and Shear on
    Flexural Motions of Isotropic Elastic Plates", J. of
    Applied Mechanics, Vol. 18, No. 1, Mar, 1951, pp 31-38.

5. Aleksandrov, E.B. and Bonch-Bruevich, A.M., "Investigation of
    Surface Strains by the Hologram Technique", Soviet Physics,
    Technical Physics (ZTF), Vol. 12, No. 2, August, 1967,
    pp 258-265.

6. Haines, K.A., and Hildebrand, B.P., "Surface Deformation
    Measurement Using the Wavefront Reconstruction Technique",
    Applied Optics, Vol. 5, No. 4, April 1966, pp 595-602.

APPENDIX

NASTRAN Program Listing

CDC 6400 SERIES
MODEL 6600

RIGID FORMAT SERIES M

LEVEL 15.2.0 (NAVY NASTRAN)

SYSTEM GENERATION DATE - 9/16/74

NASTRAN EXECUTIVE CONTROL DECK ECHO

```
ID TWISTED PLATE - NASTRAN
DIAG 14
TIME 60
CHKPNT YES
APP DISP
SOL 9,0
CEND
```

NASTRAN EXECUTIVE CONTROL DECK ECHO

ECHO OF FIRST CARD IN CHECKPOINT DICTIONARY TO BE PUNCHED OUT FOR THIS PROBLEM

RESTART TWISTED ,PLATE , 7/ 2/76, 10042,

AFAPL-TR-76-56

```
PLATE TRANSIENT RESPONSE      CASE CONTROL DECK ECHO

CARD
COUNT
  1      TITLE= PLATE TRANSIENT RESPONSE
  2      SPC=2
  3      TSTEP=60
  4      SET 2=176,165,154,143,132,121,110,99,88,77,66,55,44,33,22,11
  5        METHOD= 1
  6      SUBCASE 1
  7      SUBTITLE=HALF SINE LOAD
  8      DLOAD=70
  9      DISP=2
 10      PLOTID= FLAT PLATE / FINITE ELEMENT
 11      OUTPUT(PLOT)
 12      PLOTTER CALCOMP , MODEL 765,105
 13      SET 1= QUAD2
 14      VIEW 30.,...,89.
 15      SCALE 1.5
 16      MAXIMUM DEFORMATION .1
 17      FIND ORIGIN 1,SET 1
 18      CONTOUR ZDISP LIST .0001,.0002,.0003,.0004,.0005,.0006,.0007,
 19       0.0.8,.0055,.0061,.0015,.0025,.003,.0035,.004,.0045,
 20       .0005,.00055,.0016,.0065,.0067,.00075,.0008,.00085,
 21       .0009,.00055,.001,.00105,
 22       .00001,.00002,.00003,.00004,.00005,.00006,.00007,
 23       .0008,.00059,.0001,.0015,.0002,.00025,.003,.00035,
 24       .0004,.00045,.0005,.00055,.0006,.00065
 25      PLOT TRANSIENT DEFORMATION CONTOUR 1,TIME 1.00-6,2.10-6,SET 1,SYMBOL 0,
 26      OUTLINE
 27      CONTOUR ZDISP LIST .00001,.00002,.00003,.00004,.00005,.00006,.00007,
 28       0.00.5,.00001,.00015,.0015,.0002,.00025,.003,.0035,.004,.0045,
 29       .0005,.00055,.0006,.00065,.0067,.00075,.0008,.00085,
 30       .0009,.00095,.001,.00105,
 31       .00001,.00002,.00003,.00004,.00005,.00006,.00007,
 32       .0008,.00009,.0001,.00015,.0002,.00025,.003,.00035,
 33       .0004,.00045,.0005,.00055,.0006,.00065
 34      PLOT TRANSIENT DEFORMATION CONTOUR 1,TIME 3.90-6,4.10-6,SET 1,SYMBOL 0,
 35      OUTLINE
 36      CONTOUR ZDISP LIST .00001,.00002,.00003,.00004,.00005,.00006,.00007,
 37       0.00.5,.00001,.00015,.0015,.0002,.00025,.003,.00035,.004,.00045,
 38       .0005,.00055,.0006,.00065,.0067,.00075,.0008,.00085,
 39       .0009,.00095,.001,.00105,
 40       .00001,.00002,.00003,.00004,.00005,.00006,.00007,
 41       .0008,.00009,.0001,.00015,.0002,.00025,.003,.00035,
 42       .0004,.00045,.0005,.00055,.0006,.00065
 43      PLOT TRANSIENT DEFORMATION CONTOUR 1,TIME 5.90-6,6.10-6,SET 1,SYMBOL 0,
 44      OUTLINE
 45      CONTOUR ZDISP LIST .00001,.00002,.00003,.00004,.00005,.00006,.00007,
 46       .00006,.00009,.0001,.00015,.0002,.00025,.003,.00035,.004,.00045,
 47       .0005,.00055,.0006,.00065,.0067,.00075,.0008,.00085,
 48       .0009,.00095,.001,.00105,
 49       .00001,.00002,.00003,.00004,.00005,.00006,.00007,
 50       .00008,.00009,.0001,.00015,.0002,.00025,.003,.00035
```

55

PLATE TRANSIENT RESPONSE   CASE CONTROL DECK ECHO

```
CARD
COUNT
 51             .0004,.00045,.0005,.00055,.0006,.00065
 52     PLOT TRANSIENT DEFORMATION CONTOUR 1,TIME 7.90-6,8.10-6,SET 1,SYMBOL 0,
 53     OUTLINE
 54     CONTOUR 7DISP LIST .0001,.0002,.0003,.0004,.0005,.0006,.00007,
 55             .0006,.0001,.00015,.0002,.0025,.0003,.0004,.00045,
 56             .0005,.00055,.6,.00065,.0007,.0008,.0085,
 57             .0009,.0005,.0011,.0115,
 58             .0001,.0002,.0003,.00004,.0005,.0006,.0007,
 59             .0008,.0009,.001,.00615,.0002,.0025,.0003,.00035,
 60             .0004,.0045,.0005,.00055,.0006,.00065
 61     PLOT TRANSIENT DEFORMATION CONTOUR 1,TIME 11.9-6,12.1-6,SET 1,SYMBOL 0,
 62     OUTLINE
 63     CONTOUR 7DISP LIST .0001,.0002,.0003,.0004,.0005,.0006,.00007,
 64             .0006,.0009,.0015,.0002,.0025,.0003,.0004,.00045,
 65             .0005,.00055,.6,.00065,.0007,.0008,.0085,
 66             .0009,.0005,.001,.00105,
 67             .0001,.0002,.0003,.0004,.0005,.0006,.0007,
 68             .0008,.0009,.001,.00015,.0002,.0025,.0003,.00035,
 69             .0004,.0045,.0005,.00055,.0006,.00065
 70     PLOT TRANSIENT DEFORMATION CONTOUR 1,TIME 17.9-6,18.1-6,SET 1,SYMBOL 0,
 71     OUTLINE
 72     CONTOUR 7DISP LIST .0001,.0002,.0003,.0004,.0005,.0006,.00007,
 73             .0006,.0009,.0015,.0002,.0025,.0003,.0004,.00045,
 74             .0005,.00055,.6,.00065,.0007,.0008,.0085,
 75             .0009,.0005,.001,.00105,
 76             .0001,.0002,.0003,.0004,.0005,.0006,.0007,
 77             .0008,.0009,.001,.00015,.0002,.0025,.0003,.00035,
 78             .0004,.0045,.0005,.00055,.0006,.00065
 79     PLOT TRANSIENT DEFORMATION CONTOUR 1,TIME 23.9-6,24.1-6,SET 1,SYMBOL 0,
 80     OUTLINE
 81     CONTOUR 7DISP LIST .0001,.0002,.0003,.0004,.0005,.0006,.00007,
 82             .0006,.0009,.0015,.0002,.0025,.0003,.0004,.00045,
 83             .0005,.00055,.6,.00065,.0007,.0008,.0085,
 84             .0009,.0005,.001,.00105,
 85             .0001,.0002,.0003,.0004,.0005,.0006,.0007,
 86             .0008,.0009,.001,.00015,.0002,.0025,.0003,.00035,
 87             .0004,.0045,.0005,.00055,.0006,.00065
 88     PLOT TRANSIENT DEFORMATION CONTOUR 1,TIME 29.9-6,30.1-6,SET 1,SYMBOL 0,
 89     OUTLINE
 90     BEGIN BULK
```

*** USER INFORMATION MESSAGE 207, BULK DATA NOT SORTED,XSORT WILL RE-ORDER DECK.

PLATE TRANSIENT RESPONSE

SORTED BULK DATA ECHO

CARD COUNT	1 ..	2 ..	3 ..	4 ..	5 ..	6 ..	7 ..	8 ..	9 ..	10
1-	CQUAD2 6	1	6	17	18	18	8			
2-	CQUAD2 7	1	7	18	19	19	9			
3-	CQUAD2 8	1	8	19	20	20	9			
4-	CQUAD2 9	1	9	20	21	21	10			
5-	CQUAD2 10	1	10	21	22	22	11			
6-	CQUAD2 16	1	17	28	29	29	18			
7-	CQUAD2 17	1	18	29	30	30	19			
8-	CQUAD2 18	1	19	30	31	31	20			
9-	CQUAD2 19	1	20	31	32	32	21			
10-	CQUAD2 20	1	21	32	33	33	22			
11-	CQUAD2 26	1	28	39	40	40	29			
12-	CQUAD2 27	1	29	40	41	41	30			
13-	CQUAD2 28	1	30	41	42	42	31			
14-	CQUAD2 29	1	31	42	43	43	32			
15-	CQUAD2 36	1	32	43	44	44	33			
16-	CQUAD2 36	1	39	50	51	51	40			
17-	CQUAD2 37	1	40	51	52	52	41			
18-	CQUAD2 38	1	41	52	53	53	42			
19-	CQUAD2 39	1	42	53	54	54	43			
20-	CQUAD2 40	1	43	54	55	55	44			
21-	CQUAD2 46	1	50	61	62	62	51			
22-	CQUAD2 47	1	51	62	63	63	52			
23-	CQUAD2 48	1	52	63	64	64	53			
24-	CQUAD2 49	1	53	64	65	65	54			
25-	CQUAD2 50	1	54	65	66	66	55			
26-	CQUAD2 56	1	61	72	73	73	62			
27-	CQUAD2 57	1	62	73	74	74	63			
28-	CQUAD2 58	1	63	74	75	75	64			
29-	CQUAD2 59	1	64	75	76	76	65			
30-	CQUAD2 60	1	65	76	77	77	66			
31-	CQUAD2 66	1	72	83	84	84	73			
32-	CQUAD2 67	1	73	84	85	85	74			
33-	CQUAD2 68	1	74	85	86	86	75			
34-	CQUAD2 69	1	75	86	87	87	76			
35-	CQUAD2 76	1	76	87	88	88	77			
36-	CQUAD2 76	1	83	94	95	95	84			
37-	CQUAD2 77	1	84	95	96	96	85			
38-	CQUAD2 78	1	85	96	97	97	86			
39-	CQUAD2 79	1	86	97	98	98	87			
40-	CQUAD2 80	1	87	98	99	99	88			
41-	CQUAD2 86	1	94	105	106	106	95			
42-	CQUAD2 87	1	95	106	107	107	96			
43-	CQUAD2 88	1	96	107	108	108	97			
44-	CQUAD2 89	1	97	108	109	109	98			
45-	CQUAD2 90	1	98	109	110	110	99			
46-	CQUAD2 96	1	105	116	117	117	106			
47-	CQUAD2 97	1	106	117	118	118	107			
48-	CQUAD2 99	1	107	118	119	119	108			
49-	CQUAD2 99	1	108	119	120	120	109			
F-	CQUAD2 100	1	109	120	121	121	11			

AFAPL-TR-76-56

PLATE TRANSIENT RESPONSE

SOFTED BULK DATA ECHO

GABD COUNT	1	2	3	4	5	6	7	8	9	10
51-	CQUAD2 106		116	1	127	128	117			
52-	CQUAD2 107		117	1	128	129	118			
53-	CQUAD2 108		118	1	129	130	119			
54-	CQUAD2 109		119	1	130	131	120			
55-	CQUAD2 110		126	1	131	132	121			
56-	CQUAD2 116		126	1	138	139	128			
57-	CQUAD2 117		128	1	139	140	129			
58-	CQUAD2 118		129	1	140	141	130			
59-	CQUAD2 119		130	1	141	142	131			
60-	CQUAD2 120		131	1	149	150	139			
61-	CQUAD2 126		136	1	149	150	139			
62-	CQUAD2 127		139	1	150	151	140			
63-	CQUAD2 128		141	1	151	152	141			
64-	CQUAD2 129		141	1	152	153	142			
65-	CQUAD2 135		142	1	153	154	143			
66-	CQUAD2 136		149	1	160	161	150			
67-	CQUAD2 137		151	1	161	162	151			
68-	CQUAD2 138		151	1	162	163	152			
69-	CQUAD2 139		152	1	163	164	153			
70-	CQUAD2 145		153	1	164	165	154			
71-	CQUAD2 146		161	1	171	172	161			
72-	CQUAD2 147		161	1	172	173	162			
73-	CQUAD2 148		162	1	173	174	163			
74-	CQUAD2 149		163	1	174	175	164			
75-	CQUAD2 156		164	1	175	176	165			
76-	CQUAD2 156		171	1	182	183	172			
77-	CQUAD2 157		172	1	183	184	173			
78-	CQUAD2 158		173	1	184	185	174			
79-	CQUAD2 159		174	1	185	186	175			
80-	CQUAD2 160		175	1	186	187	176			
81-	CQUAD2 166		183	1	193	194	183			
82-	CQUAD2 167		183	1	194	195	184			
83-	CQUAD2 168		184	1	195	196	185			
84-	CQUAD2 169		185	1	196	197	186			
85-	CQUAD2 170		186	1	197	198	187			
86-	CQUAD2 176		193	1	204	205	194			
87-	CQUAD2 177		195	1	205	206	195			
88-	CQUAD2 178		196	1	206	207	196			
89-	CQUAD2 179		196	1	207	208	197			
90-	CQUAD2 180		197	1	208	209	198			
91-	CQUAD2 186		204	1	215	216	205			
92-	CQUAD2 187		205	1	216	217	206			
93-	CQUAD2 188		206	1	217	218	207			
94-	CQUAD2 189		207	1	218	219	208			
95-	CQUAD2 190		208	1	219	220	209			
96-	CQUAD2 196		215	1	226	227	216			
97-	CQUAD2 197		216	1	227	228	217			
98-	CQUAD2 198		217	1	228	229	218			
99-	CQUAD2 199		219	1	229	230	219			
100-	CQUAD2 200		219	1	230	231	220			

AFAPL-TR-76-56

PLATE TRANSIENT RESPONSE

SORTED BULK DATA ECHO.

CARD COUNT	1	2	3	4	5	6	7	8	9	10
101-	CQUAD2 266	1		226	237	238	227			
102-	CQUAD2 207	1		227	238	239	228			
103-	CQUAD2 208	1		228	239	240	229			
104-	CQUAD2 209	1		229	240	241	230			
105-	CQUAD2 216	1		236	241	242	231			
106-	CQUAD2 216	1		237	248	249	238			
107-	CQUAD2 217	1		238	249	250	239			
108-	CQUAD2 218	1		239	250	251	240			
109-	CQUAD2 219	1		240	251	252	241			
110-	CQUAD2 226	1		241	252	253	242			
111-	CQUAD2 226	1		248	259	260	249			
112-	CQUAD2 227	1		249	260	261	250			
113-	CQUAD2 228	1		250	261	262	251			
114-	CQUAD2 229	1		251	262	263	252			
115-	CQUAD2 236	1		252	263	264	253			
116-	CQUAD2 236	1		259	270	271	260			
117-	CQUAD2 237	1		260	271	272	261			
118-	CQUAD2 238	1		261	272	273	262			
119-	CQUAD2 239	1		262	273	274	263			
120-	CQUAD2 246	1		263	274	275	264			
121-	CQUAD2 246	1		271	281	282	271			
122-	CQUAD2 247	1		271	282	283	272			
123-	CQUAD2 248	1		272	283	284	273			
124-	CQUAD2 249	1		273	284	285	274			
125-	CQUAD2 256	1		274	285	286	275			
126-	CQUAD2 256	1		261	292	293	282			
127-	CQUAD2 257	1		282	293	294	283			
128-	CQUAD2 258	1		283	294	295	284			
129-	CQUAD2 259	1		284	295	296	285			
130-	CQUAD2 266	1		285	296	297	286			
131-	CQUAD2 266	1		292	303	304	293			
132-	CQUAD2 267	1		293	304	305	294			
133-	CQUAD2 268	1		294	305	306	295			
134-	CQUAD2 269	1		295	306	307	296			
135-	CQUAD2 276	1		296	307	308	297			
136-	CQUAD2 276	1		303	314	315	304			
137-	CQUAD2 277	1		304	315	316	305			
138-	CQUAD2 278	1		305	316	317	306			
139-	CQUAD2 279	1		306	317	318	307			
140-	CQUAD2 286	1		307	318	319	308			
141-	CQUAD2 286	1		314	325	326	315			
142-	CQUAD2 287	1		315	326	327	316			
143-	CQUAD2 288	1		316	327	328	317			
144-	CQUAD2 289	1		317	328	329	318			
145-	CQUAD2 296	1		318	329	330	319			
146-	CQUAD2 296	1		325	336	337	326			
147-	CQUAD2 297	1		326	337	338	327			
148-	CQUAD2 298	1		327	338	339	328			
149-	CQUAD2 299	1		328	339	340	329			
150-	CQUAD2 306	1		329	340	341	330			

AFAPL-TR-76-56

PLATE TRANSIENT RESPONSE

S O R T E D   B U L K   D A T A   E C H O

GAPD COUNT	. 1	. . 2	. . 3	. . 4	. . 5	. . 6	. . 7	. . 8	. . 9	. . 10 .
151-	CQUAD2 366	1	336	347	348	337				
152-	CQUAD2 367	1	337	348	349	338				
153-	CQUAD2 368	1	338	349	350	339				
154-	CQUAD2 309	1	339	350	351	340				
155-	CQUAD2 316	1	346	351	352	341				
156-	CQUAD2 316	1	347	358	359	348				
157-	CQUAD2 317	1	348	359	360	349				
158-	CQUAD2 318	1	349	360	361	350				
159-	CQUAD2 319	1	356	361	362	351				
160-	CQUAD2 320	1	351	362	363	352				
161-	CQUAD2 326	1	358	369	376	359				
162-	CQUAD2 327	1	359	370	371	360				
163-	CQUAD2 328	1	360	371	372	361				
164-	CQUAD2 329	1	361	372	373	362				
165-	CQUAD2 33.	1	362	373	874	363				
166-	DAREA 65	171	3	230.						
167-	EIGR 1	INV	-0	15000.	11	11				
168-	*EI MAX						6			*EI
169-	GROSET									
170-	GRID 6		.0000	.0000	.0000	.0000				
171-	GRID 7		.0000	.3000	.0000	.0000				
172-	GRID 8		.0000	.6000	.0000	.0000				
173-	GRID 9		.0000	.9000	.0000	.0000				
174-	GRID 10		.0000	1.2000	.0000	.0000				
175-	GRID 11		.0000	1.5000	.0000	.0000				
176-	GRID 17		.3000	.0000	.0000	.0000				
177-	GRID 18		.3000	.3000	.0000	.0000				
178-	GRID 19		.3000	.6000	.0000	.0000				
179-	GRID 20		.3000	.9000	.0000	.0000				
180-	GRID 21		.3000	1.2000	.0000	.0000				
181-	GRID 22		.3000	1.5000	.0000	.0000				
182-	GRID 28		.6000	.0000	.0000	.0000				
183-	GRID 29		.6000	.3000	.0000	.0000				
184-	GRID 30		.6000	.6000	.0000	.0000				
185-	GRID 31		.6000	.9000	.0000	.0000				
186-	GRID 32		.6000	1.2000	.0000	.0000				
187-	GRID 33		.6000	1.5000	.0000	.0000				
188-	GRID 39		.9000	.0000	.0000	.0000				
189-	GRID 40		.9000	.3000	.0000	.0000				
190-	GRID 41		.9000	.6000	.0000	.0000				
191-	GRID 42		.9000	.9000	.0000	.0000				
192-	GRID 43		.9000	1.2000	.0000	.0000				
193-	GRID 44		.9000	1.5000	.0000	.0000				
194-	GRID 50		1.2000	.0000	.0000	.0000				
195-	GRID 51		1.2000	.3000	.0000	.0000				
196-	GRID 52		1.2000	.6000	.0000	.0000				
197-	GRID 53		1.2000	.9000	.0000	.0000				
198-	GRID 54		1.2000	1.2000	.0000	.0000				
199-	GRID 55		1.2000	1.5000	.0000	.0000				
20.-	GRID 61		1.5000	.0000	.0000	.0000				

AFAPL-TR-76-56

PLATE TRANSIENT RESPONSE

SORTED BULK DATA ECHO

CARD COUNT	1	2	3	4	5	6	7	8	9	10
201-	GRID	62		1.5000	.3000	.0000				
202-	GRID	63		1.5000	.6000	.0000				
203-	GRID	64		1.5000	.9000	.0000				
204-	GPIC	65		1.5000	1.2000	.0000				
205-	GRID	66		1.5000	1.5000	.0000				
206-	GRID	7?		1.6500	.0000	.0000				
207-	GRID	73		1.6500	.3000	.0000				
208-	GRID	74		1.6500	.6000	.0000				
209-	GRID	75		1.6500	.9000	.0000				
210-	GRID	76		1.6500	1.2000	.0000				
211-	GRID	77		1.6500	1.5000	.0000				
212-	GPID	A3		1.8000	.0000	.0000				
213-	GRID	8?		1.8000	.3000	.0000				
214-	GRID	A5		1.8000	.6000	.0000				
215-	GRID	86		1.8000	.9000	.0000				
216-	GRID	87		1.8000	1.2000	.0000				
217-	GRID	88		1.8000	1.5000	.0000				
218-	GRID	94		1.9500	.0000	.0000				
219-	GRID	95		1.9500	.3000	.0000				
220-	GRID	96		1.9500	.6000	.0000				
221-	GRID	97		1.9500	.9000	.0000				
222-	GRID	98		1.9500	1.2000	.0000				
223-	GRID	9?		1.9500	1.5000	.0000				
224-	GRID	105		2.1000	.0000	.0000				
225-	GRID	106		2.1000	.3000	.0000				
226-	GRID	107		2.1000	.6000	.0000				
227-	GRID	108		2.1000	.9000	.0000				
228-	GPID	109		2.1000	1.2000	.0000				
229-	GRID	110		2.1000	1.5000	.0000				
230-	GRID	116		2.2500	.0000	.0000				
231-	GRID	117		2.2500	.3000	.0000				
232-	GPID	118		2.2500	.6000	.0000				
233-	GPID	119		2.2500	.9000	.0000				
234-	GRID	120		2.2500	1.2000	.0000				
235-	GPID	121		2.2500	1.5000	.0000				
236-	GRID	127		2.4000	.0000	.0000				
237-	GPID	128		2.4000	.3000	.0000				
238-	GRID	129		2.4000	.6000	.0000				
239-	GPID	130		2.4000	.9000	.0000				
240-	GRID	131		2.4000	1.2000	.0000				
241-	GPID	132		2.4000	1.5000	.0000				
242-	GPID	138		2.5500	.0000	.0000				
243-	GRID	139		2.5500	.3000	.0000				
244-	GRID	140		2.5500	.6000	.0000				
245-	GPID	141		2.5500	.9000	.0000				
246-	GRID	142		2.5500	1.2000	.0000				
247-	GRID	143		2.5500	1.5000	.0000				
248-	GRID	149		2.7000	.0000	.0000				
249-	GRID	150		2.7000	.3000	.0000				
250-	GPID	151		2.7000	.6000	.0000				

61

PLATE TRANSIENT RESPONSE

SORTED BULK DATA ECHO

CARD COUNT		1	2	3	4	5	6	7	8	9	10
251-	GRID	152			2.7500	.9000	.0000				
252-	GRID	153			2.7000	1.2000	.0000				
253-	GRID	154			2.7000	1.5000	.0000				
254-	GRID	160			2.8500	.0000	.0000				
255-	GRID	161			2.8500	.3000	.0000				
256-	GRID	162			2.8500	.6000	.0000				
257-	GRID	163			2.8500	.9000	.0000				
258-	GRID	164			2.8500	1.2000	.0000				
259-	GRID	165			2.8500	1.5000	.0000				
260-	GRID	171			3.0000	.0000	.0000				
261-	GRID	172			3.0000	.3000	.0000				
262-	GRID	173			3.0000	.6000	.0000				
263-	GRID	174			3.0000	.9000	.0000				
264-	GRID	175			3.0000	1.2000	.0000				
265-	GRID	176			3.0000	1.5000	.0000				
266-	GRID	182			3.1500	.0000	.0000				
267-	GRID	183			3.1500	.3000	.0000				
268-	GRID	184			3.1500	.6000	.0000				
269-	GRID	185			3.1500	.9000	.0000				
270-	GRID	186			3.1500	1.2000	.0000				
271-	GRID	187			3.1500	1.5000	.0000				
272-	GRID	193			3.3000	.0000	.0000				
273-	GRID	194			3.3000	.3000	.0000				
274-	GRID	195			3.3000	.6000	.0000				
275-	GRID	196			3.3000	.9000	.0000				
276-	GRID	197			3.3000	1.2000	.0000				
277-	GRID	198			3.3000	1.5000	.0000				
278-	GRID	204			3.4500	.0000	.0000				
279-	GRID	205			3.4500	.3000	.0000				
280-	GRID	206			3.4500	.6000	.0000				
281-	GRID	207			3.4500	.9000	.0000				
282-	GRID	208			3.4500	1.2000	.0000				
283-	GRID	209			3.4500	1.5000	.0000				
284-	GRID	215			3.6000	.0000	.0000				
285-	GRID	216			3.6000	.3000	.0000				
286-	GRID	217			3.6000	.6000	.0000				
287-	GRID	218			3.6000	.9000	.0000				
288-	GRID	219			3.6000	1.2000	.0000				
289-	GRID	220			3.6000	1.5000	.0000				
290-	GRID	226			3.7500	.0000	.0000				
291-	GRID	227			3.7500	.3000	.0000				
292-	GRID	228			3.7500	.6000	.0000				
293-	GRID	229			3.7500	.9000	.0000				
294-	GRID	230			3.7500	1.2000	.0000				
295-	GRID	231			3.7500	1.5000	.0000				
296-	GRID	237			3.9000	.0000	.0000				
297-	GRID	238			3.9000	.3000	.0000				
298-	GRID	239			3.9000	.6000	.0000				
299-	GRID	240			3.9000	.9000	.0000				
300-	GRID	241			3.9000	1.2000	.0000				

PLATE TRANSIENT RESPONSE

SORTED BULK DATA ECHO

CARD COUNT	.	1	..2	..3	..4	..5	..6	..7	..8	..9	..10
361	GRID	242		.0000	3.0000	1.5000	.0000				
362	GRID	248			4.0500	.0000	.0000				
363	GRID	249			4.0500	.3000	.0000				
364	GRID	250			4.0500	.6000	.0000				
365	GRID	251			4.0500	.9000	.0000				
306	GRID	252			4.0500	1.2000	.0000				
367	GRID	253			4.0500	1.5000	.0000				
308	GRID	259			4.2000	.0000	.0000				
309	GRID	260			4.2000	.3000	.0000				
310	GRID	261			4.2000	.6000	.0000				
311	GRID	262			4.2000	.9000	.0000				
312	GRID	263			4.2000	1.2000	.0000				
313	GRID	264			4.2000	1.5000	.0000				
314	GRID	270			4.3500	.0000	.0000				
315	GRID	271			4.3500	.3000	.0000				
316	GRID	272			4.3500	.6000	.0000				
317	GRID	273			4.3500	.9000	.0000				
318	GRID	274			4.3500	1.2000	.0000				
319	GRID	276			4.3500	1.5000	.0000				
320	GRID	281			4.5000	.0000	.0000				
321	GRID	282			4.5000	.3000	.0000				
322	GRID	283			4.5000	.6000	.0000				
323	GRID	284			4.5000	.9000	.0000				
324	GRID	285			4.5000	1.2000	.0000				
325	GRID	286			4.5000	1.5000	.0000				
326	GRID	292			4.8125	.0000	.0000				
327	GRID	293			4.8125	.3000	.0000				
328	GRID	294			4.8125	.6000	.0000				
329	GRID	295			4.8125	.9000	.0000				
330	GRID	296			4.8125	1.2000	.0000				
331	GRID	297			4.8125	1.5000	.0000				
332	GRID	303			5.1250	.0000	.0000				
333	GRID	304			5.1250	.3000	.0000				
334	GRID	305			5.1250	.6000	.0000				
335	GRID	306			5.1250	.9000	.0000				
336	GRID	307			5.1250	1.2000	.0000				
337	GRID	308			5.1250	1.5000	.0000				
338	GRID	314			5.4375	.0000	.0000				
339	GRID	315			5.4375	.3000	.0000				
340	GRID	316			5.4375	.6000	.0000				
341	GRID	317			5.4375	.9000	.0000				
342	GRID	318			5.4375	1.2000	.0000				
343	GRID	319			5.4375	1.5000	.0000				
344	GRID	325			5.7500	.0000	.0000				
345	GRID	326			5.7500	.3000	.0000				
346	GRID	327			5.7500	.6000	.0000				
347	GRID	328			5.7500	.9000	.0000				
348	GRID	329			5.7500	1.2000	.0000				
349	GRID	330			5.7500	1.5000	.0000				
350	GRID	336			6.0625	.0000	.0000				

PLATE TRANSIENT RESPONSE   SORTED BULK DATA ECHO

```
CARD
COUNT    .   1  ..  2  ..  3   ..   4    ..   5   ..   6   ..   7   ..   8   ..   9   .. 10 .
351-  GRID  337              6.6625      .3000       .0000
352-  GRID  338              6.6625      .6000       .0000
353-  GRID  339              6.6625      .9000       .0000
354-  GRID  340              6.0625     1.2000       .0000
355-  GRID  341              6.6625     1.5000       .0000
356-  GRID  7.7                          .0000       .0000
357-  GRID  348              6.3750      .3000       .0000
358-  GRID  349              6.3750      .6000       .0000
359-  GRID  350              6.3750      .9000       .0000
360-  GRID  351              6.3750     1.2000       .0000
361-  GRID  352              6.3750     1.5000       .0000
362-  GRID  358              6.6975      .0000       .0000
363-  GRID  359              6.6875      .3000       .0000
364-  GRID  360              6.6475      .6000       .0000
365-  GRID  361              6.6475      .9000       .0000
366-  GRID  362              6.6875     1.2000       .0000
367-  GRID  363              6.6875     1.5000       .0000
368-  GRID  369              7.0000      .0000       .0000
369-  GRID  370              7.0000      .3000       .0000
370-  GPID  371              7.0000      .6000       .0000
371-  GRID  372              7.0000      .9000       .0000
372-  GRID  373              7.0000     1.2000       .0000
373-  GRID  374              7.0000     1.5000       .0000
374-  MAT1   1     1.+7      .3          .2587E-3
375-  PARAM LMODES 10
376-  SPC1   1     1         .1875
377-  SPC1   2     4    17    20    39    50    61    72   +A2
378-  +A2   83    94   105   116   127   138   149   160   +32
379-  +B2  171   182   193   204   215   226   237   248   +C2
380-  +C2  259   276   261   292   303   314   325   336   +D2
381-  +D2  347   350   369
382-  SPC1   2  123456   6   THRU   11
383-  TABLED1 75
384-  +A75  0.0       0.17C5    6.0-6   9.0-6                              +A75
385-  +A75  12.0-6  15.0-6  0.7557  18.0-6  0.8563  21.0-6  0.9319         +B75
386-  +C75  24.0-6  27.0-6  0.9996  27.5-6  1.0000  28.0-6  0.9996         +C75
387-  +D75  31.0-6  34.0-6  0.9319  37.0-6  0.8563  40.0-6  0.7557         +E75
388-  +E75  43.0-6  46.0-6  0.4917  49.0-6          52.0-6  0.1705         +F75
389-  +F75  55.0-6  0.1000  ENDT
390-  TLOAD1 70    65                  75
391-  TSTEP  60    55     1.0-6    1
      ENDDATA
```